DESIGN OF AN AUTOMATED CALIBRATION

DEVICE FOR ELECTROMAGNETIC TRACKING SYSTEMS

By

GARETH DOUGLAS COLE

A thesis submitted in partial fulfillment of
The requirements for the degree of

MASTER OF SCIENCE IN MECHANICAL ENGINEERING

WASHINGTON STATE UNIVERSITY
School of Mechanical and Materials Engineering

MAY 2007

To the Faculty of Washington State University:

The members of the Committee appointed to examine the thesis of GARETH DOUGLAS COLE find it satisfactory and recommend that it be accepted.

_____

Chair

_____

_____

ACKNOWLEDGEMENTS

I would like to thank all of the people that have played a major role in helping me complete this research, as well as provided support in other ways during my time here at Washington State. This thesis is dedicated to my wife Cara and our son Evan, without whom I would never have had the ambition or desire to obtain an advanced degree. Also, to our baby daughter who will be new to this world at about the same time I graduate.

I would like to thank my advisor Dr. Sankar Jayaram and Dr. Uma Jayaram for allowing me to participate in the activities of the VRCIM Lab and providing guidance during my thesis work. I also want to thank my committee member Dr. Chuck for being my favorite professor as an undergraduate student, finally tying together the endless memorization and technical formulas into a real life design project. I want to thank my lab-mate Hrishikesh Kate for helping me with the design and construction of this device, and for driving across the state with me in a WSU van to install it with sixteen foot framing lashed on top. Thank you to Sanjay Gowda and Roglenda Repp, previous VRCIM lab members, for providing the foundation for this project with their research into calibration methods. I would also like to thank Youngjun Kim and Okjoon Kim for always being willing to help me with their invaluable programming skills.

DESIGN OF AN AUTOMATED CALIBRATION DEVICE FOR ELECTOMAGNETIC TRACKING SYSTEMS

Abstract

By Gareth Douglas Cole, M.S.
Washington State University
May 2007

Chair: Sankar Jayaram

Electromagnetic tracking systems used in virtual reality applications are subject to tracking error due to magnetic field distortions caused by metallic objects in the environment which increases with increased distance from the transmitter. These problems can lead to a significant decrease in tracking performance of position and orientation during simulations in the virtual environment, creating a need for a calibration method of the tracking system. The calibration method involves collecting a set of data pairs for the receiver using the electromagnetic system and a secondary reference system of true physical locations. The goal of this research was to design a suitable device to automatically collect data points for this physical reference system without causing further distortion to the magnetic field. The calibration device was designed in order to accurately position the electromagnetic receiver at user-specified grid points throughout the tracking environment, thereby allowing the calculation of position and orientation error at each location.

The calibration device we designed is a three axis Cartesian positioner interfaced via serial port with computer software for an automated methodology. The main

components of the device are two perpendicular eight foot lead screw driven rails for x-y translation, with a descending nylon telescoping arm for z translation. The entire device is mounted to overhead framing and the main components are fixed to a smaller frame that can be translated; this allows for a calibration over a wide range of physical locations. The stepper motors that drive the axis' are controlled via the Calibration of Virtual Environment (COVE) software, which allows the user to specify the calibration bounds as well as the resolution for each direction. Novel methods were created to avoid collision of the calibration device with objects in the environment.

The device was installed and tested at a sponsor's facility. Data was collected and analyzed for calibration of the facility. The tests showed that the density of calibration and the flexibility achieved with this device far exceed any previous methods used.

TABLE OF CONTENTS

LIST OF FIGURES

1. INTRODUCTION

1.1 Virtual Reality

Virtual reality describes an interactive artificial environment simulated by a computer system. It has been defined as: a computer simulation of a real or imaginary system that enables a user to perform operations on the simulated system and shows the effects in real time [1]. This environment is displayed in an immersive three dimensional form allowing for depth perception, thereby providing a more realistic and intuitive experience as opposed to using a traditional two dimensional screen. Virtual reality can be adapted to many uses: engineering environments such as a factory floor assembly line, medical training procedures for sensitive surgical operations, military applications such as battlefield training, or simulated environments for gaming.

Most virtual reality systems utilize a head-mounted display (HMD) for immersing the user in the environment. The HMD has two screens, one for each eye, that display offset images to allow for stereoscopic viewing to provide depth perception. A tracking system is needed in conjunction with the HMD to allow physical movements to be translated to movement in the virtual environment by updating the graphical display when the head is moved.

Standard input devices such as a keyboard and mouse can be used to interact with the environment, or more application specific hardware can be utilized. A sensor embedded glove, such as the CyberGlove® from Immersion Corporation, is a hardware device that relays angular data corresponding to the hand motion of the user [2]. This

hand can be graphically displayed in the virtual environment and can facilitate the manipulation and grasping of objects for assembly purposes.

To further enhance the virtual experience, haptics devices can be incorporated to simulate the physical surroundings. An example of a portable haptics device is the CyberGrasp® system, from Immersion Corporation, that uses a mechanical exoskeleton to apply resistive force feedback to the user's hand to represent a virtual object's physical geometry when grasped [2]. If coupled with a CyberForce®, also from Immersion Corporation, the user can get a very realistic sensation of an object's weight and inertial properties. The CyberForce uses a large mechanical linkage that attaches to the hand to provide translational forces; this linkage also doubles as a tracking system because shaft encoders on the linkage relay position and orientation of the hand. This complex haptics system can be extremely useful in virtual reality simulations but is prohibitive in both its very high cost as well as a restricted range of motion and added bulk to the user. One very popular and basic haptics device is the PHANToM, from SensAble Devices Co. [3]. The PHANToM is restricted to a small range of motion and must be mounted to a desk surface. It generates forces on a pen shaped object that allow the user to feel physical properties of a virtual object such as surface texture, stiffness, and basic geometry.

1.2 Tracking Systems

A tracking system is used as a key component of virtual reality systems, providing the position and orientation of dynamic objects in the environment. Tracking systems generally output the position and orientation of an object using six variables: three

translational (x, y, and z) and three rotational (yaw, pitch, and roll). The main object to be tracked is the head, allowing an update of the scene when the user looks around at his or her surroundings. Most tracking systems support multiple sensors, enabling tracking of multiple components of the user's movements. There are many different types of tracking systems, each with their own strengths and weaknesses. The tracking system chosen is therefore based on the specific needs of the virtual reality application. This field is rapidly progressing with the advancement of wireless technologies, further reducing the current restrictions on freedom of movement.

To provide an immersive experience in real-time, a tracking system must update quickly to present a realistic view of the virtual environment. Therefore, latency in the position and orientation update must be very small in order to refresh the graphics of tracked objects or viewpoints. Another critical component of tracking systems is accuracy: the coordinates of a tracked object must be calculated to within millimeters of the physical location for optimum performance. The necessary accuracy for the tracking system is ultimately application specific; ergonomics reviews, for example, require an accuracy of 1 mm or less. The tracking system must also be designed such that no motion, or "jitter", occurs in the scene while the user is standing still and such that small movements lead to small changes in tracker output. Finally, mobility is very important for tracking systems because restrictions on the user further reduce the virtual experience.

There are four main types of tracking systems currently in use: mechanical, optical, acoustic, and electromagnetic. A brief discussion of each system with its associated advantages and disadvantages will be reviewed.

Mechanical:

Mechanical tracking systems use a series of linkages connected to the tracked object and relay position and orientation through kinematical methods. Mechanical systems are extremely accurate but are restrictive in their range of motion and additional weight added to the user.

Optical:

Optical tracking systems use video cameras usually in conjunction with Light Emitting Diodes (LEDs). A software algorithm scans the image of the LEDs from each camera in order to triangulate a three dimensional location in space. Multiple cameras are used because a line of sight is required at all times for the tracked points. Optical systems are very useful because the user is not restricted by any wires or cables, and is becoming increasingly cost effective with the advent of new camera technology.

Acoustic:

Acoustic tracking systems use ultrasonic frequencies to determine position and orientation. Acoustic sensors are often used in a hybrid tracking system; they incorporate inertial sensors to determine orientation. These systems have a longer lag time and are generally unreliable due to error generated with changing room temperature and humidity as well as interference from echoes and other outside noise.

Electromagnetic:

Electromagnetic tracking systems use a stationary transmitter that generates a magnetic field. This field can be either generated using a pulsed DC current such as the Flock of Birds from Ascension Technologies [4] or by an AC current like the Polhemus

FASTRAK system [5]. Mobile receivers calculate the strength of this stationary magnetic field to determine their respective position and orientation relative to the transmitter. These systems are effective for large areas and are very suitable for engineering applications but suffer from distortion and noise induced by other magnetic fields from electronics as well as eddy currents generated from metal in the environment. The Flock of Birds from Ascension Technologies is pictured below in Figure 1.1.

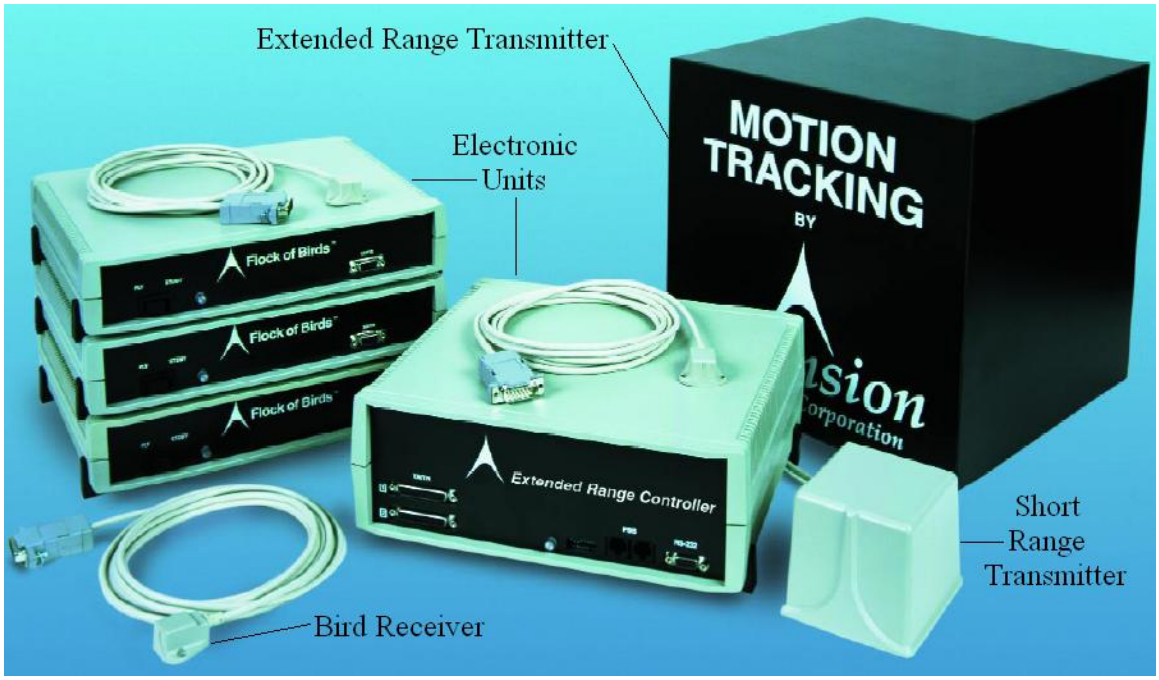

Figure 1.1: Flock of Birds Electromagnetic Tracking System

2. BACKGROUND

2.1 Flock of Birds Electromagnetic Tracking System

The tracking system used in the VRCIM laboratory is the Flock of Birds manufactured by Ascension Technologies [4]. The Flock of Birds is an electromagnetic orthogonal tracking system that uses a pulsed DC signal to determine position and orientation. A transmitter generates electromagnetic signals which are received by a sensor. The strengths of the electromagnetic signals are used to determine the absolute position and orientation of the receiver relative to the transmitter. This tracking system allows a wide range of motion but suffers from decreasing accuracy with distance from the transmitter. The manufacturer's specifications state an accuracy of ±1.8 mm for position and ±0.5º RMS for orientation; however this is only verified for distances from 20.3 cm up to 76.2 cm. Therefore, the system is very precise up to approximately 2.5' but has increasingly unpredictable results as distance increases to the 10' maximum range.

The electromagnetic transmitter has three orthogonal coils which are pulsed in sequence. The receiver also contains three orthogonal coils which measure the components of the electromagnetic signal. The strengths of the three components of the received pulse are compared to the strength of the transmitted pulse to determine the position. The strength of the three received signals are compared to each other to determine the orientation (thus the receiver coil most parallel to the transmitter coil will give the highest value and the one most orthogonal will give the lowest). For each position component, the transmitter sends three pulses, one for each of its coils.

Therefore the receiver gets a total of nine signals in order to calculate the x, y, and z components of position; from these nine signals the orientation is inferred.

There are three available models for the Flock of Birds: a short-range transmitter (±2 feet), mid-range transmitter (±4 feet), and an extended-range transmitter (±10 feet). The extended range transmitter is the one used for this research, and allows tracking within a ten foot radius from the transmitter. Unfortunately, the accuracy of the system is negatively affected by many sources. Accuracy decreases markedly as distance from the sensor to the transmitter increases due to a weakened magnetic field strength. The signal is also distorted by interference from external noise and metallic distortion present in the environment.

In order to fully understand the magnetic field created by a pulsed DC signal, as is the case with the tracking system, one must look at time-dependent fields, as described by the set of four Maxwell's equations. Numerical or analytical methods can be used to solve this system of Maxwell's equations provided a set of initial and boundary conditions. In order to solve a complex system involving several material regions, such as the tracking environment, Maxwell's equations are solved in each material region to determine the electromagnetic field. The field is assumed to be continuous and to have continuous first partial derivatives in each region. With these assumptions, one can establish relationships that the electromagnetic field must satisfy at a given material boundary. These relationships are called electromagnetic boundary conditions. Electromagnetic boundary conditions are not the typical form of boundary conditions because they do not specify a field on a given boundary surface, they specify "jumps" that must occur in components of the field when crossing a material boundary. These

“jumps” are due to induced surface charges or surface currents created in various materials by the electromagnetic radiation from the source.

The transmitter used in the Flock of Birds tracking system is set to take 86 to 106 measurements per second, nominally. One can reduce error caused by metal in the environment by reducing the measurement rate. This is because high frequency measurements actually create eddy currents in non-ferrous metals which disrupt the signal. Eddy currents are swirling electrical currents created inside a conductive material in the presence of a changing magnetic field. These currents distort the magnetic field and contribute to error in position and orientation output. While this effect is much more prominent in AC tracking systems, it is still significant in DC systems such as the Flock of Birds because of the alternating flux created from the “on-off” pulsing generation of the magnetic field.

Ferrous metals in the environment create further complications due to an induced magnetizing field [6]. The magnetizing field is produced due to the high permeability of such metals. The amount of distortion in the magnetic field increases with an increase in both the geometric size as well as the permeability of the metal. This effect tends to diminish with increasing transmitter frequency, and is therefore more prevalent in DC systems such as the Flock of Birds. The magnetizing effect of ferrous metals is the single most significant source of error for DC electromagnetic tracking systems.

Now that one can understand the basics of the strength of a given magnetic field at various locations in space, it is critical to understand how the receiver in a magnetic tracking system is able to determine its position and orientation based on the transmitter. As previously stated, three coils inside the receiver each get a signal from the three coils

in the transmitter. This signal transmission is based on Faraday's Law of Induction:

$$Emf = -N\frac{\partial \phi}{\partial t}$$

where the voltage induced in a coil is equal to the number of turns in the coil times the change in flux with respect to time. As the coils in the magnetic transmitter are pulsed, they emit a magnetic field that produces a varying flux that induces a voltage in each of the receiver coils, a phenomenon known as mutual inductance. These three voltage signals are amplified and then filtered before being sent via serial port to a data acquisition system. The computer can then compare the strength of each signal to determine position and orientation.

Comprehending the mathematics involved in the electromagnetic system allows for a more intuitive approach to a tracking error solution. From the differential equations that define the strength of a magnetic field, it is apparent that the resulting flux will be extremely varied throughout a large tracking environment such as the eight foot radius for the Flock of Birds. While the magnetic permeability of air is relatively low, it will have an increasing effect on the retention of the signal as distance from the transmitter increases; at extended distances a lower strength field will reduce accuracy. Also, eddy currents are created by a high frequency of the magnetic flux inside of conductive metals in the tracking workspace that induce error by distorting the uniform magnetic field. Ferrous metals in the environment create an induced magnetized field and further distort the signal. As distance increases from the transmitter more metallic objects will compound this effect and greatly magnify the overall error. Removing any unnecessary metal will improve performance, but is not practical for many engineering applications.

Metals with very large mass such as I-beams in the floor or walls also cause distortion, and are impossible to remove. While the generated distortion may be significant, it can be accounted for because its measurement is repeatable and the error is therefore static

2.2 Calibration Methodology

Calibrating a tracking system involves mapping a distorted tracker reading to its associated true location in space. This requires the simultaneous collection of tracker data along with the corresponding physical measurement data for pre-defined locations. These two sets of data allow the generation of an error vector field (the returned positions subtracted from the actual positions) for the tracking space. From this data, an algorithm can be applied in order to correct the static distortion for the tracker readings at any arbitrary location in the calibrated space.

Location error correction techniques can be classified into two categories: *global methods* that take all points into account to derive an appropriate global mapping function, and *local methods* that use only some points to obtain a localized solution [7]. This research only utilizes a local method for obtaining a corrected tracker reading; no attempt has been made to obtain a global mapping function as the calibrated space is assumed to have any number of metallic obstructions that will create a very non-uniform error field.

Previous research has been completed in order to implement a software program using C/C++ to correct the tracking readings as they are recorded. Correcting the readings in real time involves some computational overhead which reduces the overall

measurement rate. This reduction is generally insignificant due to existing limitations on the graphical refresh rate for engineering applications. The main components of the methodology are outlined in Figure 2.1:

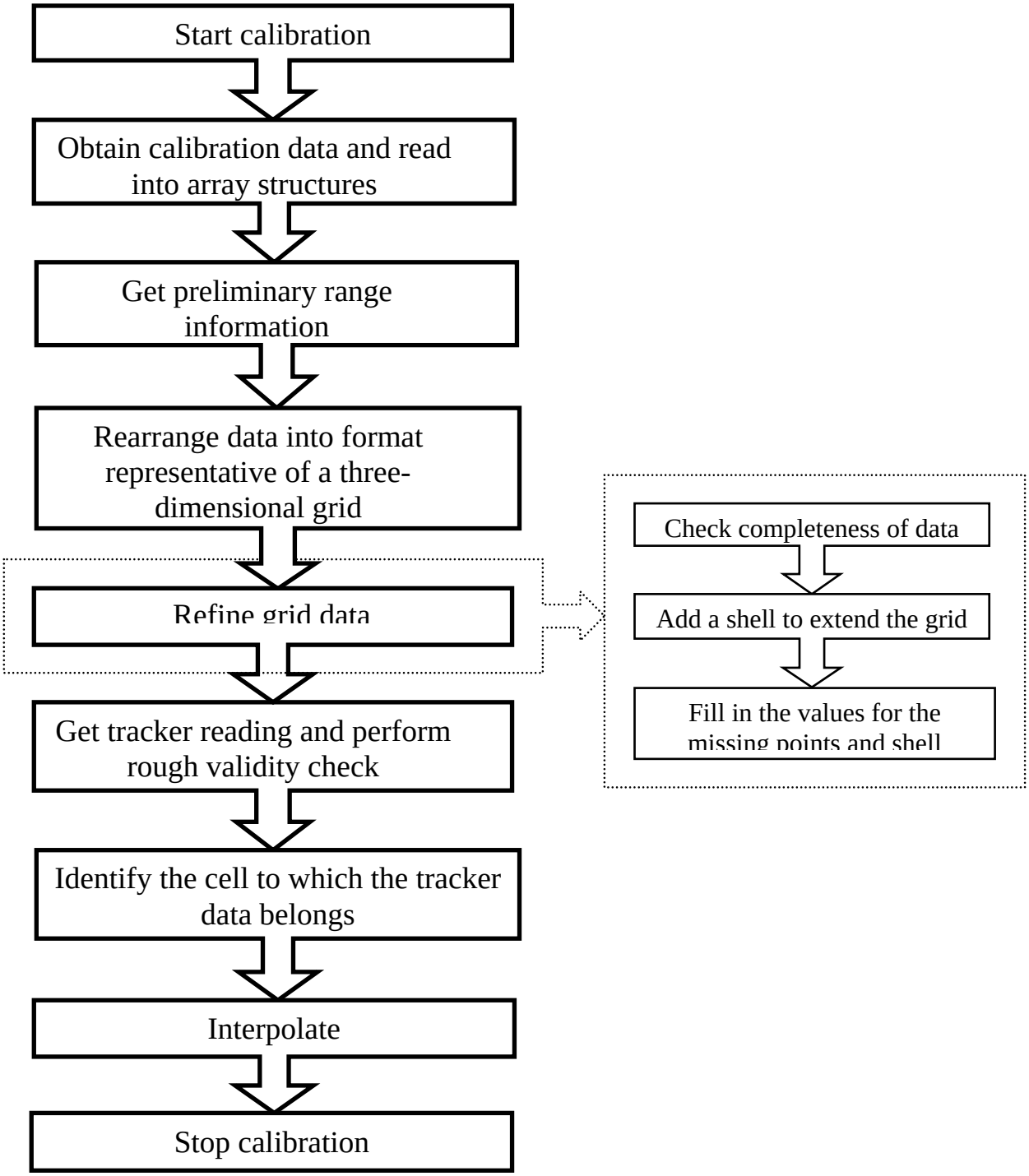

Figure 2.1: Outline of the Calibration Process [8]

There are three main steps in the correction process [8]:

1. Read the calibration grid data points from a file and preprocess the data. The position and orientation components, virtual and physical, for all of the points in the grid are stored in a data file. The program reads the information for the data points and transfers them into a data structure.

2. Search the grid for the cell containing the tracker reading. Take a reading from the tracker and search the cells in the grid, using the information in the data structure created in step 1. The search terminates when a cell is found such that its volume contains the tracker point, or after the last cell is searched. If a bounding cell is not located, the tracker point is outside of the calibrated volume.

3. Interpolate the eight vertices of this cell to obtain the corrected data. If the tracker point resides in one of the cells, then use the eight vertices of that particular cell to perform an interpolation and correct the distorted tracker reading.

The interpolation of the vertices is a very important step in the calibration process, as there are many methods to accomplish this. It was found through extensive case studies that affine tetrahedral mapping produces the best results. Affine tetrahedral mapping involves mapping a distorted volume to its corresponding physical volume; mapping the tracker readings to the physical coordinates. An explanation is as follows [9]:
"For this calibration method, the tetrahedrons are used instead of the cells. For each tracker reading, two independent transformations are performed once the encompassing

tetrahedron is identified. The first one maps the virtual position tetrahedron to the physical position tetrahedron and the second maps the virtual positions to the virtual orientations. Although the same virtual position tetrahedron is mapped to both the virtual orientation and the physical position tetrahedrons, this provides a distinct transformation for the two different distortion fields."

2.3 Calibration of Virtual Environment

The Calibration of Virtual Environment (COVE) software has been developed at WSU and is an integral part of the calibration procedure. COVE uses a data density procedure for real-time error correction in distorted tracking environments; a higher calibration data density reduces the maximum residual error (distortion remaining after calibration). The Graphical User Interface (GUI) allows the user to define a region for calibration by setting the minimum and maximum x, y, and z values as well as the number of data points per axis. Sub-regions can also be defined if the user wishes to calculate a higher density of points in a given subdivision of the region. This software has been developed further in the scope of this research to allow integration with the calibration device for automated measurement acquisition and collision detection.

The COVE system consists of five basic functional modules, shown in the flowchart in Figure 2.2 and outlined below [10]:

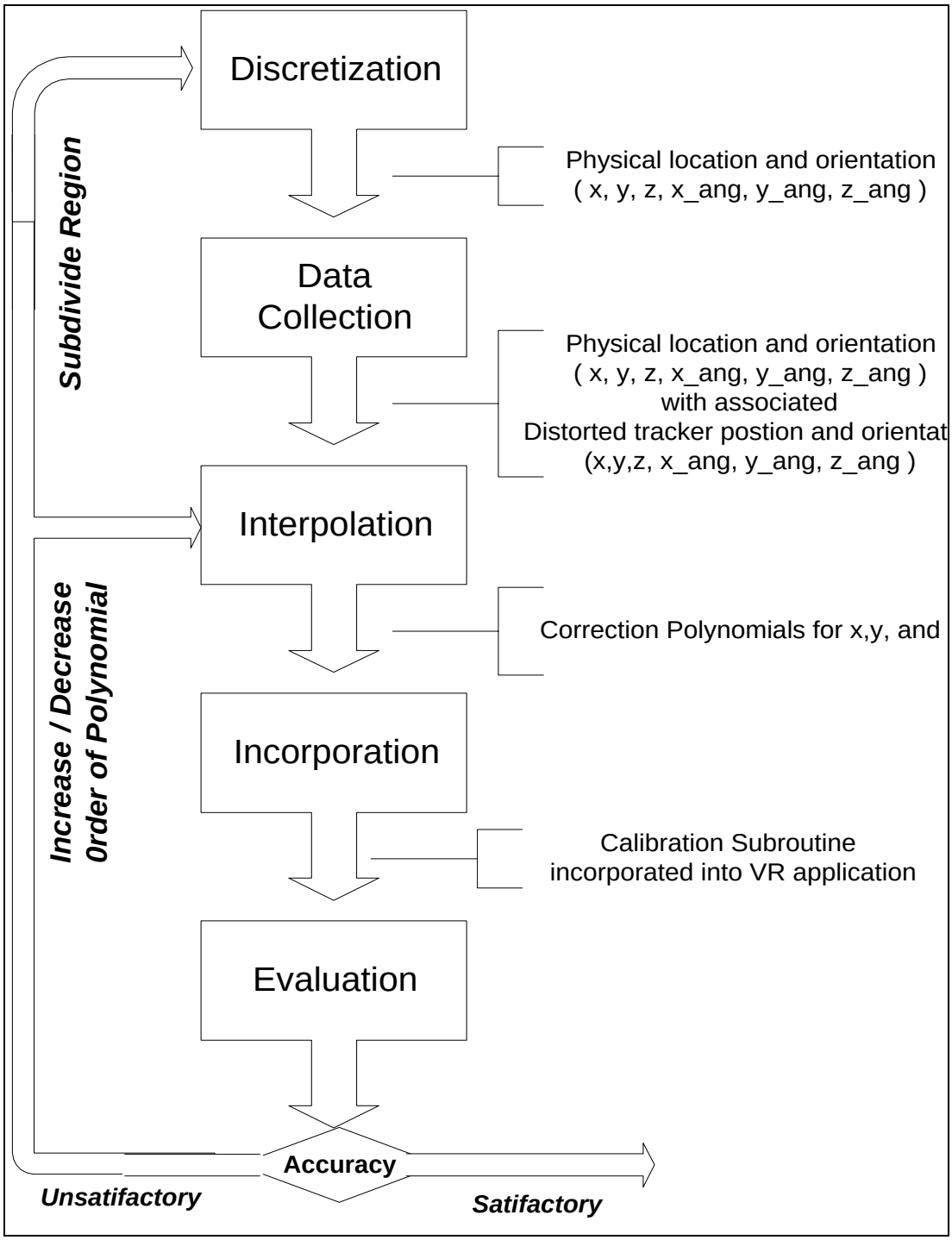

Figure 2.2: COVE Components [10]

1. Discretization - The physical environment volume where the VR application will be performed is defined as a rectangular box shaped region. This volume is divided into smaller rectangular hexahedrons of uniform size, hereafter referred to as cells. The collective vertices of these cells create a 3D Cartesian grid of data points. The grid density of the calibration space is a measure indicating the number of points per unit volume. The higher the region density, the more detailed the calibration becomes, and subsequently the lower the residual error. Ideally, an infinite number of points could be measured, leading to a minimum residual error. Obviously this is not a practical solution and the trade-off between time and accuracy must be considered.

2. Data Collection - At each grid point in the virtual environment, the location and orientation are recorded, both physical and virtual. The tracker is accurately placed with zero orientation at a known location using a mechanical measuring device. These comprise the physical positions and orientations. The corresponding virtual position and orientation data are obtained by taking the distorted electromagnetic x, y, and z coordinates and the yaw, pitch, and roll angles of the tracker. The information is stored in a file, with each line containing the nine data components for a single point.

3. Interpolation - The static distortion at a specific calibration point is the difference between the mechanically measured physical position of the receiver and the electromagnetically measured virtual position. This applies to the orientation as well.

The physical and virtual positions and orientations are interpolated, providing a mapping from the distorted virtual data to the desired physical data.

4. Incorporation – The interpolation methods must be incorporated into the application. When a tracker reading is taken for use in an application, it is interpolated using the virtual and physical grid data to obtain the corrected position and orientation. The corrected tracker data is then used in the VR software.

5. Evaluation - An evaluation of the results can help minimize residual error remaining after the calibration. A visualization of the residual error vector field is commonly used in order to observe any regions of the workspace that may need to be calibrated more accurately.

3. LITERATURE REVIEW

3.1 Overview

There have been many research projects focused on the calibration of electromagnetic tracking systems. A majority of this research has focused almost entirely upon the correction algorithm itself, with little thought given to the physical data collection. As the scope of this research is the design of an automated calibration device for data collection, only measurement procedures for calibration will be reviewed. The calibration methods can be divided into two main categories:

- Manual Measurement Calibration Devices
- Automated Measurement Calibration Devices

3.2 Manual Measurement Calibration Devices

A majority of calibration research has involved the manufacturing of some sort of wooden or plastic stand that can be moved around in the environment, requiring a tedious process of physically moving the stand to various locations throughout the tracking space. As this method is time consuming, a large spacing is generally required in the grid locations due to time constraints. Large grid spacing in the calibration method is a disadvantage because each calibrated position during tracker use must be interpolated

from a wide range of data points.

The first research project involving the calibration of an electromagnetic tracking system was conducted at the NASA AMES Research Center in 1992 [11]. In order to collect their data set, they constructed a 6'x4' pegboard on a stand. This pegboard contained holes at 12" intervals to fix the receiver location; at each location, sixty data points were recorded in order to filter out noise from the Polhemus tracking system. After collecting each data point the receiver was moved to the next position and the process repeated. The floor was marked with positions so that an 8'x8'x6' volume could be measured.

A plastic vertical stand with a sliding mount was machined from acrylic and aligned along a plotted floor grid by Gowda [10]. The receiver was mounted to a dove-tail slider and used a fixed measuring tape for reading the z position, allowing any number of data points from 1" to 75" from the floor. Set-screws were incorporated to ensure an orientation with zero-pitch and zero-yaw. The accuracy of this device relied on the machining tolerances of the acrylic stand as well as the precision used in positioning the stand at a particular (x, y, z) coordinate. The calibration was performed in an environment cleared of all unnecessary metals or electronics. The data collection process was extremely time-consuming requiring a decision on the tradeoff between time and accuracy.

A manual calibration was performed while purposefully placing a metallic truck seat between the receiver and tracker by Repp [8]. The intent of this intended distortion was to verify the benefits of calibration for tracking ergonomic engineering applications with static (repeatable) error. A three tiered acrylic calibration stand was machined to

allow for a 7x7x3 mesh of stations to which the tracking device could be attached using plastic screws, shown in Figure 3.1. The stations were spaced 1.6033 inches in both the x and y directions for an overall calibration space of 9.6198 x 9.6198 x 12.000 inches, for a maximum of 147 points in the grid. This process utilized a very fine grid spacing for good accuracy, but the calibrated region was very small in perspective of the full range of the tracking device. This problem was noted, "*For a virtual reality application the entire virtual space should be calibrated as densely as possible. This is extremely time consuming and is viable with computer assisted or robotic data collection but impractical for one person to calibrate*." [8]

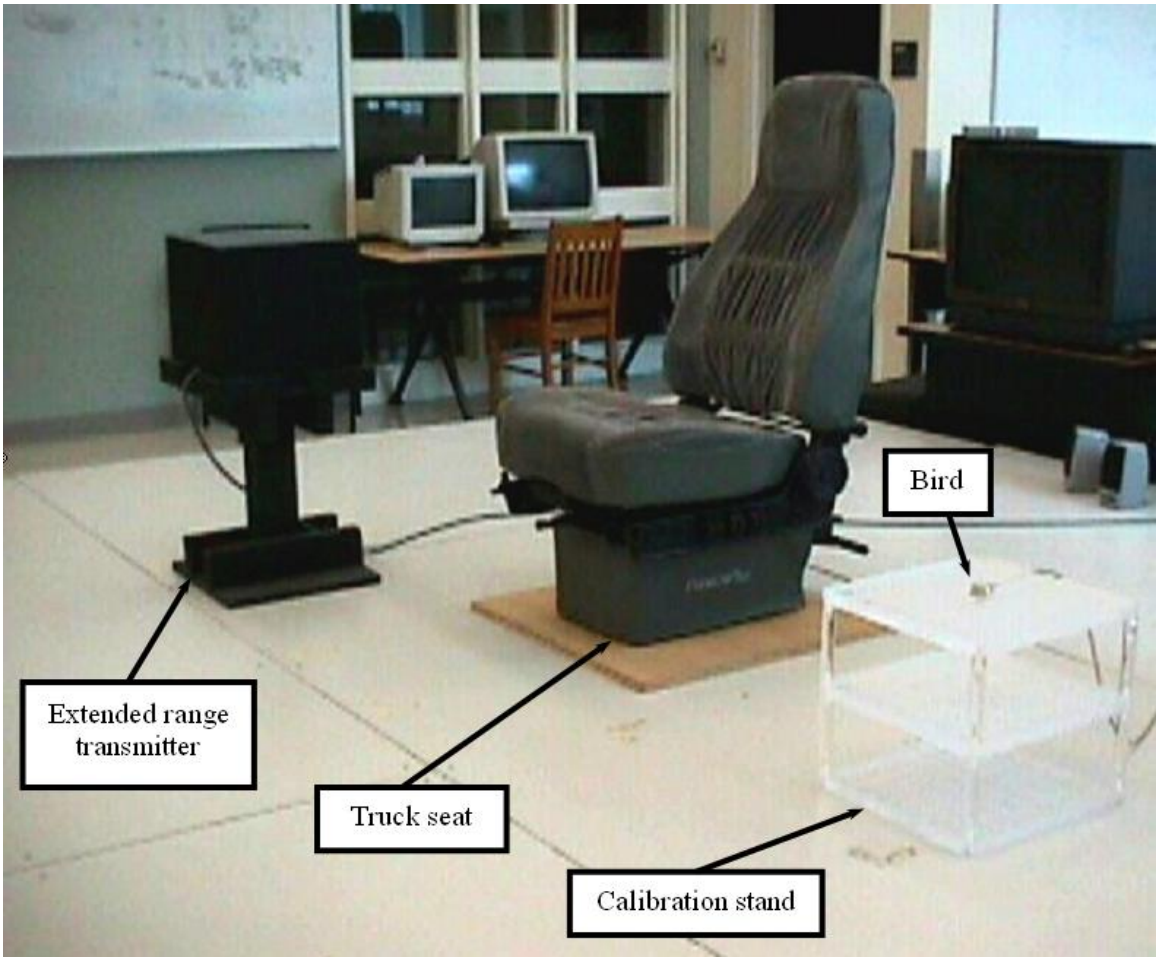

Figure 3.1: Manual Calibration with Static Distortion [8]

Another variation of the plastic stand calibration was performed for the National Institute of Standards and Technology, Mathematical and Computational Sciences Division [12]. A grid was projected onto the floor to aid in positioning plastic crates, from an office supply store, shown in Figure 3.2. Due to the large size of the stand, only an array of 7x6x6 measurement points was possible for the entire tracking space. The bird was either directly fixed to the top or mounted inside of a plastic cube for interchangeable orientations.

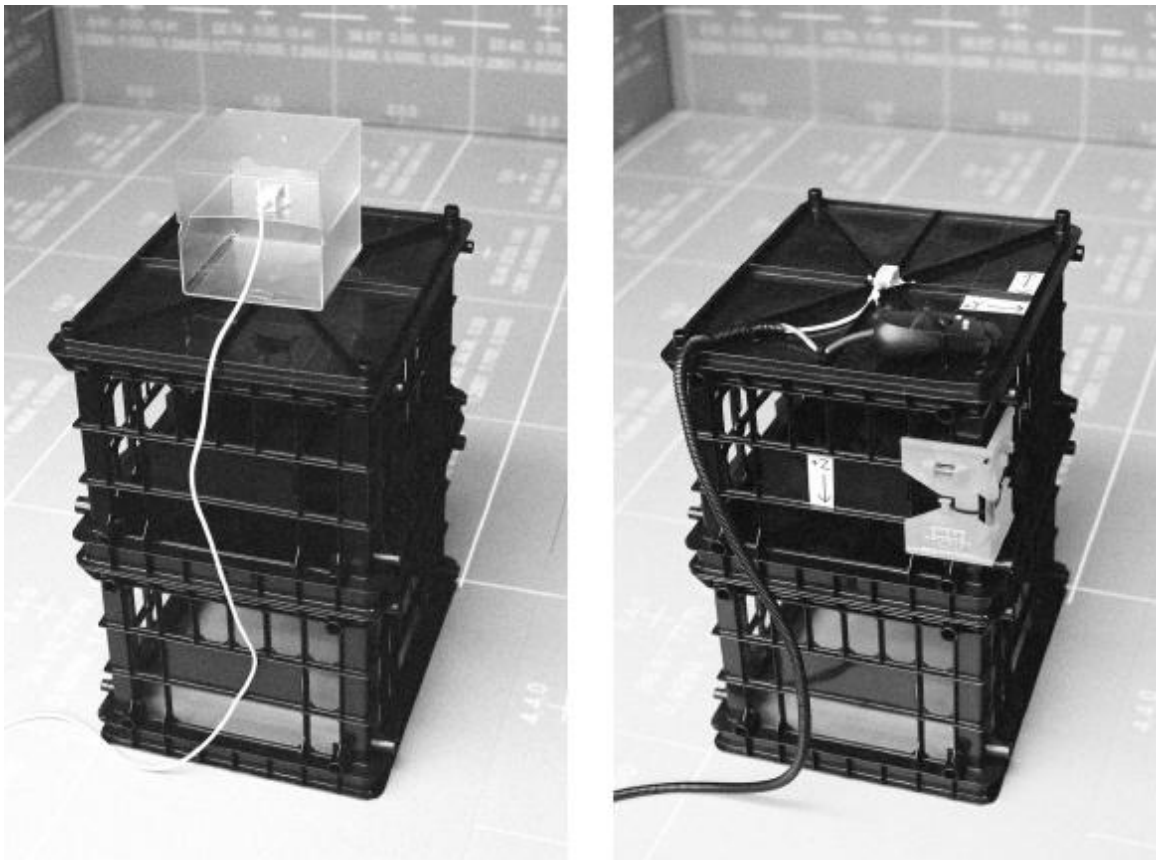

Figure 3.2: NIST Crate Calibration with Projected Grid [12]

The most creative approach to a manual measurement calibration device is presented by Borst [13]. A LEGO panel was mounted to a frame to create a 24.6 x 16.4 x

8.2 inch calibration grid size. The panel was mounted vertically on a grooved base to allow it to slide back a forth to provide readings a third dimension. Only a small calibration environment was needed because they were using the Ascension MiniBird, which is a smaller form of the Flock of Birds with a lower transmitter range. Their calibration algorithm required two orientation positions for each location, with the bird attached inside of a small LEGO cube seen below in Figure 3.2.

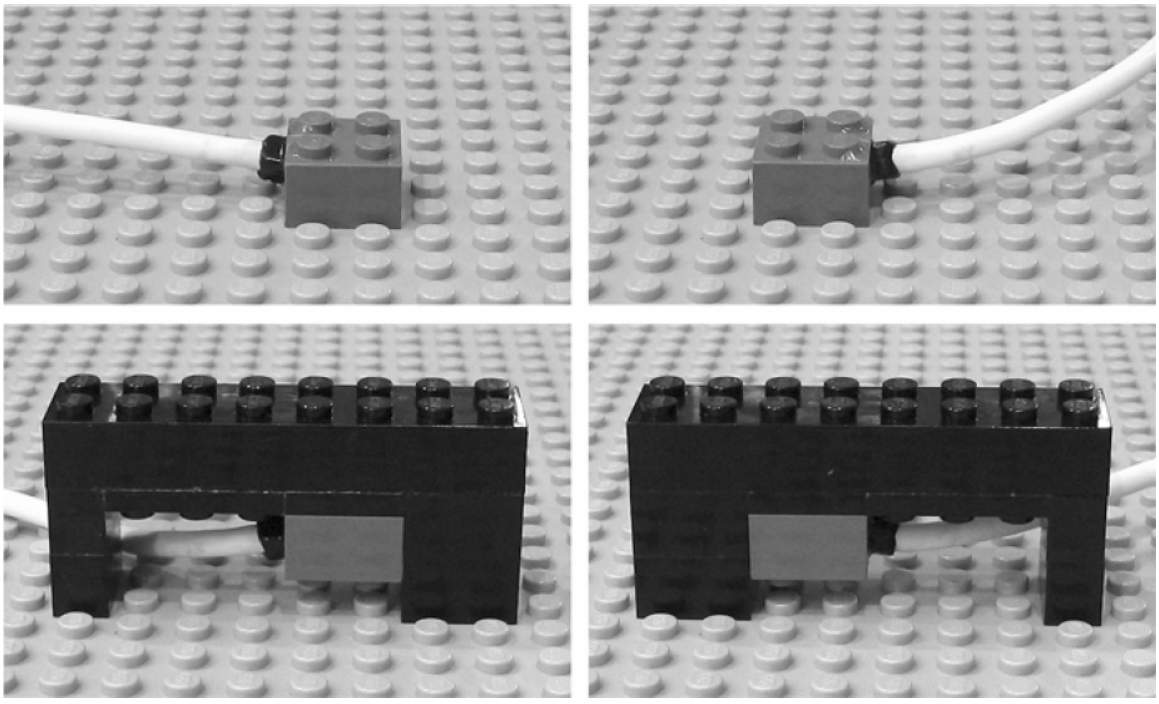

Figure 3.3: LEGO Calibration Device Orientations [13]

3.3 Automated Measurement Calibration Devices

An ultrasonic measuring device (UMD) was used by Ghazisaedy to provide an automated physical location measurement to calibrate an electromagnetic tracking system

inside of a CAVE environment [14]. The CAVE is a 10'x10'x10' virtual reality system that uses rear projected screens to display the stereoscopic images on the surrounding walls as well as the floor, eliminating the need for a head-mounted display. A UMD generates an ultrasonic sound signal from a transducer that is reflected off of an object; the elapsed time for the signal to be emitted and returned (the echo) is directly proportional to the distance. Four UMDs were mounted to the receiver: one to measure the distance to the ground (z), one to measure the distance to the front of the CAVE (y), and two to measure the distance to each wall (x). Two UMDs were used for the x measurement to verify that the yaw orientation was zero; if the additive distance of the two measurements was equal to the total distance of ten feet from wall-to-wall the yaw was considered to be aligned properly. Mercury switches were used to verify that the pitch and roll was within ten degrees of normal, if the degree was greater than ten the system would not record data. A very interesting concept for this calibration method is that the calibration was performed by a user inside of the immersive environment; data points to be taken were portrayed as interactive three-dimensional cubes. Once the bird was inside of the cube, within a certain tolerance, a measurement was taken and the cube changed color to depict completed locations. The accuracy of this system was dependent on the overall accuracy of the UMD measurement of approximately 1.8 inches. This measurement accuracy was determined to be suitable due to the distortions of up to four feet, at the maximum transmitter range of ten feet, before calibration. This method works very well inside of a uniform tracking environment with equally spaced walls, such as the CAVE, but would not be suitable for head-tracking applications in an engineer's office location.

A six degree of freedom mechanical arm was used to calibrate an electromagnetic system by Livingston [15]. The mechanical tracking system was a commercially available product, the Metrecom IND-01 from Faro Technologies, Inc. The Faro arm uses aluminum mechanical linkages with hybrid digital-analog rotary transducers to yield extremely accurate positional accuracies of 0.46 mm over a 1.8 m radius sphere. A 0.3 m plastic tip was attached to the measurement location of the arm in order to provide some "buffer" distance from the metallic components. A depiction of the measurement device along with its associated transformation to the Flock of Birds coordinate system is shown in Figure 3.4. This calibration device requires manual positioning by the user, making it a very time-intensive calibration process.

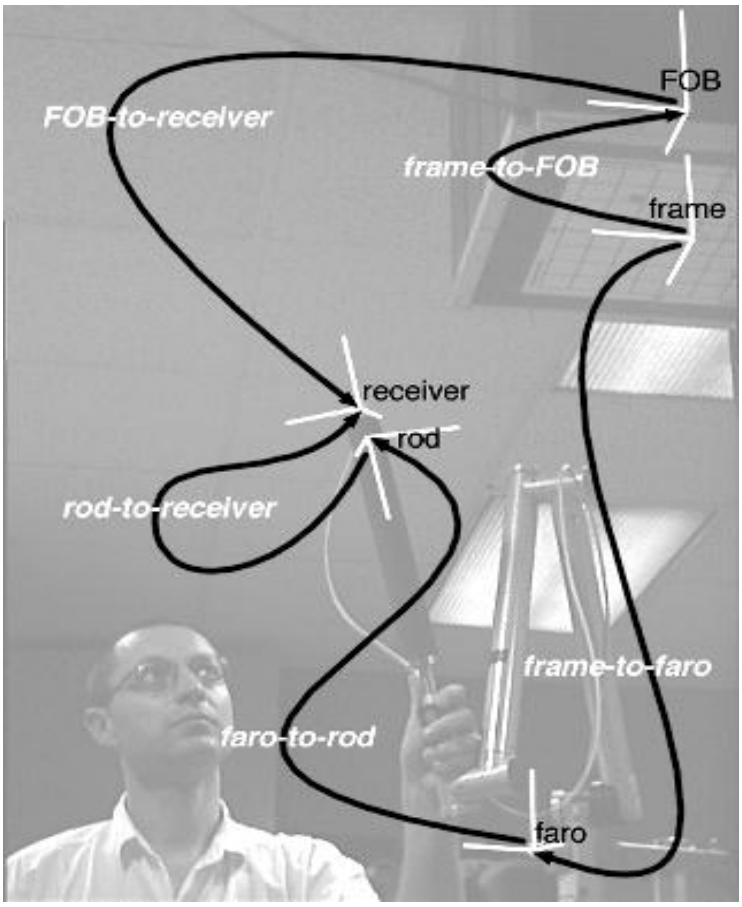

Figure 3.4: Mechanical Tracking System Calibration [15]

A combination of a manually positioned calibration apparatus with an optical position measurement was designed at the Scientific Computing and Imaging Institute at the University of Utah [16]. The NDI Optotrak 3020 was used as the optical tracking system, which has a nominal accuracy for the infrared markers of 0.05 mm per meter of distance along the central focal axis. A plastic mounting apparatus was manufactured from plastic pipes to position the bird arbitrarily at any location and orientation, with six infrared markers fixed as seen in Figure 3.5. The infrared markers were positioned positively and negatively along orthogonal axes so that three markers were visible to the camera regardless of receiver orientation. This method allowed the calibration stand to be positioned very quickly, as the location of the bird was completely reliant on the optical tracking system camera. This system is very accurate but prohibitive in its manual positioning of the receiver as well as extremely high cost (~$60,000 for the Optotrak).

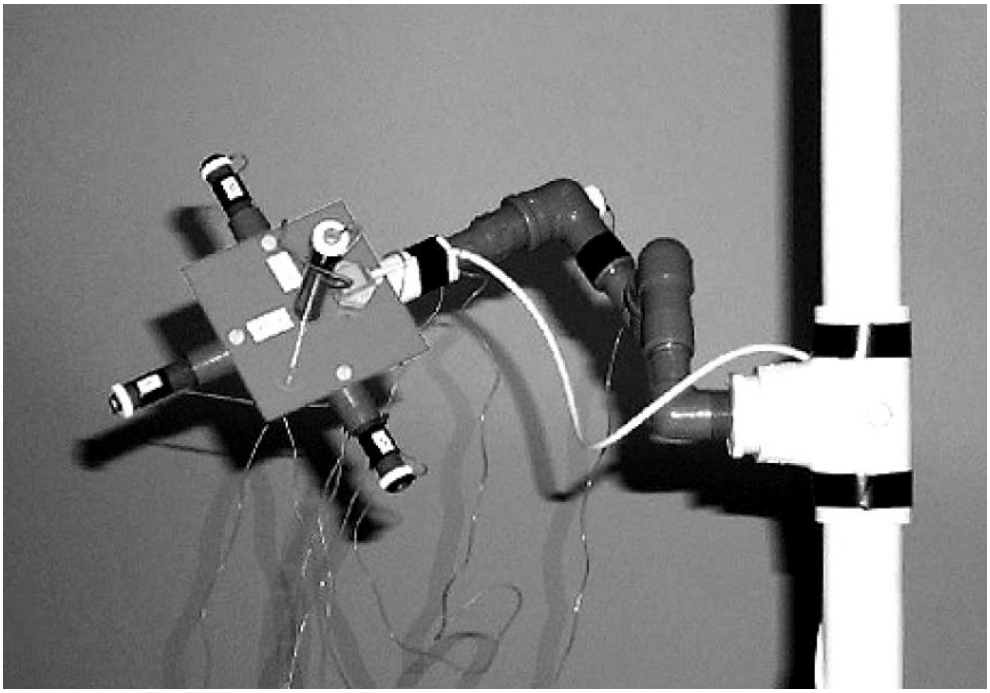

Figure 3.5: Calibration Stand with Infrared Markers [16]

4. PROBLEM STATEMENT AND SCOPE OF RESEARCH

Electromagnetic tracking systems used for virtual reality applications provide a very good reference frame for engineering applications but suffer from position and orientation errors caused by magnetic field distortion. Metals in the tracking space may cause significant distortion but this can be accounted for because the generated error is static: its measurement is repeatable as long as the environment remains unchanged. A calibration can be performed by accurately positioning the receiver at known locations in the tracking space while taking associated tracker readings to generate data pairs. These data pairs can be used to generate a three-dimensional array of error vectors as a function of position at each calibration point. Error vectors can be used to interpolate tracker readings in real-time in order to account for and correct the error present in the magnetic field. The results from a calibration are dependent on the number of data points taken. More data points allow for a smaller range of surrounding error vectors for interpolation, which yields a higher accuracy and better resolution for engineering applications. Previous calibration methods have been dependent on a very time-intensive process of manually positioning the receiver, limiting the amount of data available for error correction. This research proposes the design of a device to automatically position the receiver at user-specified locations without causing further distortion to the magnetic field. The research consists of four phases:

1) Preliminary Research

Preliminary research was performed in the field of automated data collection. A prototype calibration device was constructed using a borrowed three axis traverse; this device allowed a small-scale calibration of a two foot cube. From this preliminary research, much was learned about the requirements and challenges associated with constructing a full-scale automated calibration device.

2) Design and Manufacture of the Automated Calibration Device

Specifications for the design of an automated calibration device have been received from the project sponsor, PACCAR Inc. These specifications will be reviewed and from this key needs defined in order to generate concepts. A design is to be chosen in order to meet the necessary accuracy and material specifications. Vendors are to be contacted and bids received for the selection of the major components. Upon completion of the design assembly in the VRCIM laboratory, testing is to be performed to ensure that the device meets the necessary performance specifications.

3) Integration of the Calibration Device with COVE

In order to automate the data collection process, the calibration device will be integrated with the existing COVE software. COVE must communicate with the calibration device in order to position the receiver at the user defined g rid points. This will require COVE to output corresponding motor commands to achieve the necessary translations.

4) Implementation of Collision Avoidance

The final phase of the research is to implement collision avoidance with static obstructions in the calibration region. The collision avoidance is required to be easily modified for various tracking environments with different obstructions. This ensures that a tracking environment with common static objects such as a chair or even the transmitter itself will not be collided with by the calibration device during automated data collection.

5. PRELIMINARY RESEARCH

5.1 Prototype Design

As a basis for a prototype, a three-axis traverse was borrowed from another laboratory. This traverse was entirely metallic in construction. In order to use the traverse to collect data, it was necessary to design and fabricate a nonmetallic stand off arm. The traverse was placed on a four foot by four foot auxiliary stage in one corner of the main VR stage. Since the traverse only covers a range of x = 24 inches, y = 10 inches, and z = 25 inches, a sliding extension was created for the stand off arm so that the y-axis could cover a full 24 inch range without having to move the entire device. One PC was used to the position the traverse at the specified grid points while the COVE program was operated on a separate PC. The existing COVE capabilities were not modified for this phase of the project; manual input of the physical tracker location into the GUI was required while the program simultaneously recorded the bird position. The tracker data was received by an SGI Octane II visual workstation and put into table format in an XML file that was sent over the lab network to the computer running COVE via shared memory.

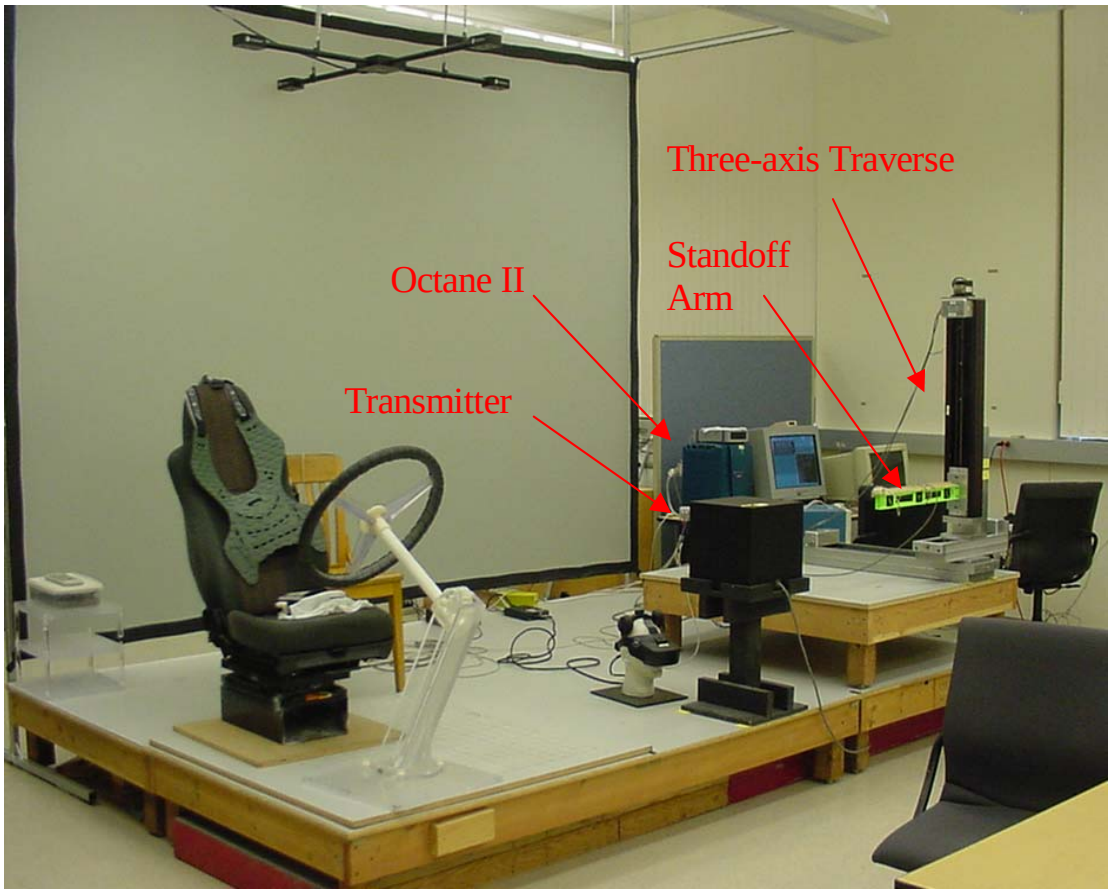

Figure 5.1: Prototype Overview

Figure 5.1 shows an overview of the VRCIM lab with the test apparatus installed. The main stage is 12'x8', and is raised one foot from the building floor to get away from any interference that might be caused by any metal (rebar, conduit, etc.) incorporated in the floor structure. The traverse was set on an auxiliary stage so that the 2 foot cube to be calibrated would cover the range of motions made by a standing man. Figure 5.2 shows the three-traverse axis, and the stand off beam. The stand off beam was intended to position the bird away from any interference caused by the metal and current carrying cables of the traverse. Due to time constraints (i.e., the traverse was only available for one week), the stand off beam was based on a commercial two foot carpenter's level

made entirely from plastic. The level was attached to an aluminum plate, Figure 5.3, which was in turn mounted on the z-axis carriage. A sliding extension had a bird holder mounted on its end, Figure 5.4. This extension enabled data points to be gathered spanning two feet in the y direction without moving the traverse.

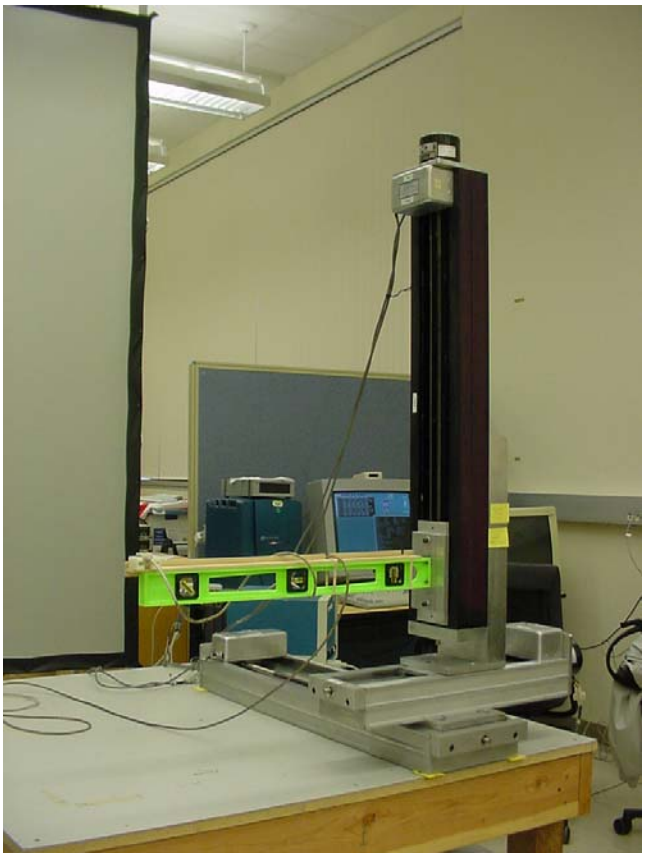

Figure 5.2: Calibration Device

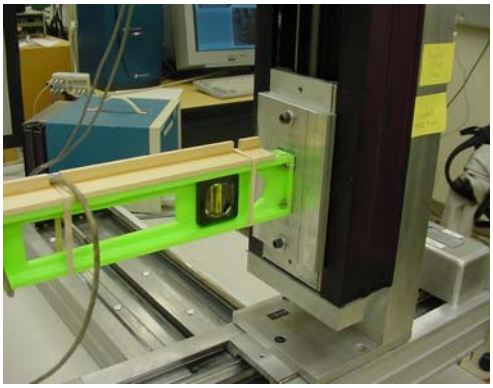

Figure 5.3: Aluminum Fixture

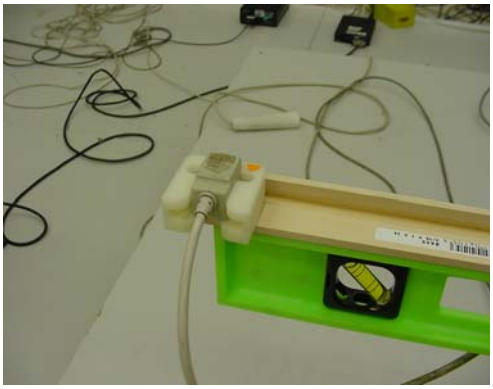

Figure 5.4: Bird Mount

Both the transmitter and the traverse were leveled using a Starrett precision level provided by John Grimes in the Dana machine shop, shown in Figure 5.5. Post-it notes were used as shims under each corner of the transmitter stand and the traverse. The paper shims provided fine enough adjustments such that it was possible to level both stand and traverse to within 0.001inches per foot, or to within 0.005º of level. The plastic beam

extension visibly deflected when an attempt was made to use the precision level on the long axis; however, the non-precision level already built into the carpenter's level was used as a secondary verification.

Figure 5.5: Precision Level

Each axis of the traverse has a stepper motor that moves its associated carriage in the x, y, or z direction. It takes 200 step commands to produce one revolution of the motor shaft, and the shaft is coupled to a lead screw with a pitch of 20 threads per inch. Thus one step advances the carriage 0.00025 inches, well within the 0.01 inch accuracy target for this prototype. The stepper motor controller associated with the traverse had motion commands sent to it from a PC in the VRCIM lab using a Quick Basic program written by Robert Lentz for use in another experiment. One operator was required to send commands to the traverse while a second operator acquired the bird position in the COVE program from the electromagnetic tracking system.

5.2 Data Collection Methods

After the apparatus was set up, data collection began. A lattice of test points in COVE was created that matched the planned moves by the traverse. Each plane of the lattice was covered by traversing the x-axis in 3-inch increments while traversing the z-axis 3-inches to a new position at each end of the x-axis. At every location, one person read the physical location from the PC controlling the stepper motors, while the other person recorded the location into the COVE GUI which simultaneously collected the electromagnetic tracker location. When all the data points on one plane were collected, the y-axis was advanced 3-inches to a new plane and the process was repeated. This process took seven hours to collect data for the designated 2 foot cube region.

5.3 Results and Conclusions

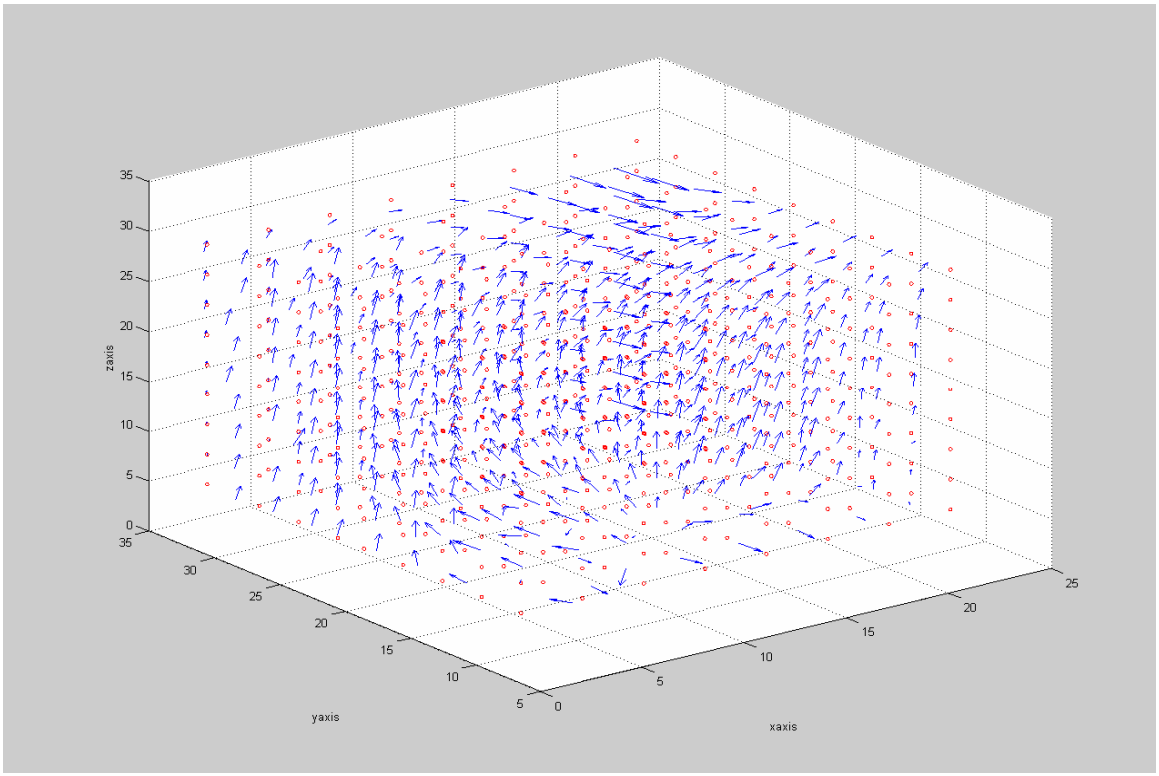

Figure 5.6: Preliminary Calibration Results

Figure 5.6 is a plot of the error vectors produced from the 729 point data set collected for the electromagnetic tracking system. The traverse was positioned at the origin of the axis, at the bottom of the figure. The red circles denote the traverse positions, and the length of the arrows is proportional to the position error. The directions of the arrows reflect the angular errors in roll, pitch, and yaw. The three angular errors were combined using direction cosines for this plot.

As seen in Figure 5.6, when the bird was closest to the traverse the directions of the arrows are very chaotic compared to when the bird was farther away. This leads to the conclusion that the 2-foot stand off arm was not long enough to separate the traverse (composed primarily of steel, a ferrous and conductive metal) from the receiver. The error vector directions appear to be uniform at 3 feet from the traverse, so at least that length of arm is recommended for future tests using a similar traverse.

The main conclusion from this prototype testing was that the motor controller commands needed to be integrated with COVE. The procedure of having one person control the physical position from the PC communicating with the stepper motors while another person manually input the data into COVE was extremely tedious and time consuming.

6. Design and Manufacture of the Calibration Device

6.1 Device Specifications

This research project was sponsored by PACCAR Inc., with the end goal that the device would be installed for use at their technical center in Mt. Vernon, WA. Craig Palmer, our company contact, devised the following specifications for the calibration system:

1. Measurement Accuracy - 1 mm or less position, 0.1 degree or less orientation. The position and orientation measurement accuracy should vary within +/- 5% of values taken at all other points in the device measurement range.
2. Measurement Volume – a tracked space within a 10-foot radius from the MotionStar Extended Range Transmitter is desired. To calibrate the space containing the 10-foot radius hemisphere is the end goal. The first choice is a calibration device that can calibrate the entire region at once (requiring the device to be set up only once) with the measurement accuracy given in 1). Otherwise, the measurement volume of the device should be large enough to minimize the number of setups required to measure the 10-foot radius hemisphere space while meeting the measurement accuracy requirements.
3. Measurement Time - It is desired that the time to measure the 10-foot radius hemisphere tracking space not exceed 4 hours.

4. Materials - The calibration device should be constructed of materials that do not affect the measurement field for the MotionStar. The calibration device must not introduce measurement error into the calibration procedure due to the presence of metal or motors that significantly influence the tracking space electromagnetic field.
5. Setup and Take-Down Time - It is desired that the calibration device be able to be setup in 20 minutes or less, and taken down in 20 minutes or less.
6. Software Integration - The calibration device must interface with the COVE calibration software (April 2005 version) to automate the data collection of region and sub-region points.
7. Obstacles in the Environment -
    - Define regions in COVE
    - Consider proximity sensors in the calibrated space

From these specifications key needs were identified in order to generate concepts:

- Materials: The most important factor in the design of the calibration device was the fact that the materials it was manufactured from could not further distort the magnetic field. This severely restricted the components available for use.
- Accuracy: The 1mm accuracy requires a very precise method for positioning the receiver.

- Cost: While not listed on the specifications from PACCAR, the project budget proved to be crucial in the overall design. An extremely precise design for the calibration device would be worthless if the required components were too expensive to acquire.

6.2 Design Considerations

The possible concepts for this design were very limited due to the very constricting specifications for accuracy and materials. Robotic "pick and place" arms were considered, but they were eliminated due to the extensive use of metal in their components. Custom building a non-metallic robot to move about the environment would not be feasible with the very tight accuracy requirement over such an extended travel distance. It quickly became obvious that a gantry crane design would be necessary to provide a buffer distance between the main positioning components of the device and the receiver taking positional measurements.

From our experience with the prototype calibration device, it was decided that purchasing a commercially available traverse would be the best solution for the required accuracy of the receiver position. There are many companies the market two and three axis positioners but most of these are for very small traverse lengths on the order of one to two feet with extremely high resolution. As the desired measurement volume consisted of a ten foot radius from the MotionStar transmitter a custom built device was required. This large dimension created many problems in terms of economics as well as accuracy due to deflection. One consideration was to construct a smaller device that

could be moved around on a rigid frame to cover the entire measurement volume in quadrants.

As all commercially available positioners are constructed of metal it was decided that a two axis positioner could be mounted overhead and then a third nonmetallic arm would descend to provide non-influenced measurement readings. The calibration device would have three motors, one for each axis, and either be servo or stepper driven. These motors can be controlled using either a special PCI card with individual components (power supply, amplifier, etc.) or with a single motion controller package provided by various companies. These motion controllers vary by manufacturer and have different programs but generally they are capable of controlling all three axes one at a time via serial port commands.

We received a number of quotes from automation companies for this two axis positioner but most estimates were outside of the range for the project budget. After extensive contact with multiple companies, we narrowed the field down to three vendors. Due to the high price of the linear actuators, a sole source justification was necessary. This memo was written to describe to our purchasing department the reason we chose H2W Technologies as the manufacturer. This memo details the other quotes we had received and the various issues with accuracy and control (Appendix A).

6.3 Final Design Components

The calibration device constructed consists of five major components (Figure 6.1):

- Lead screw driven linear actuators for x-y translation

- Linear bearing for support
- Motor controller for communication via serial port
- Telescoping arm and drive system
- Bosch-Rexroth framing for mounting and quadrant translation

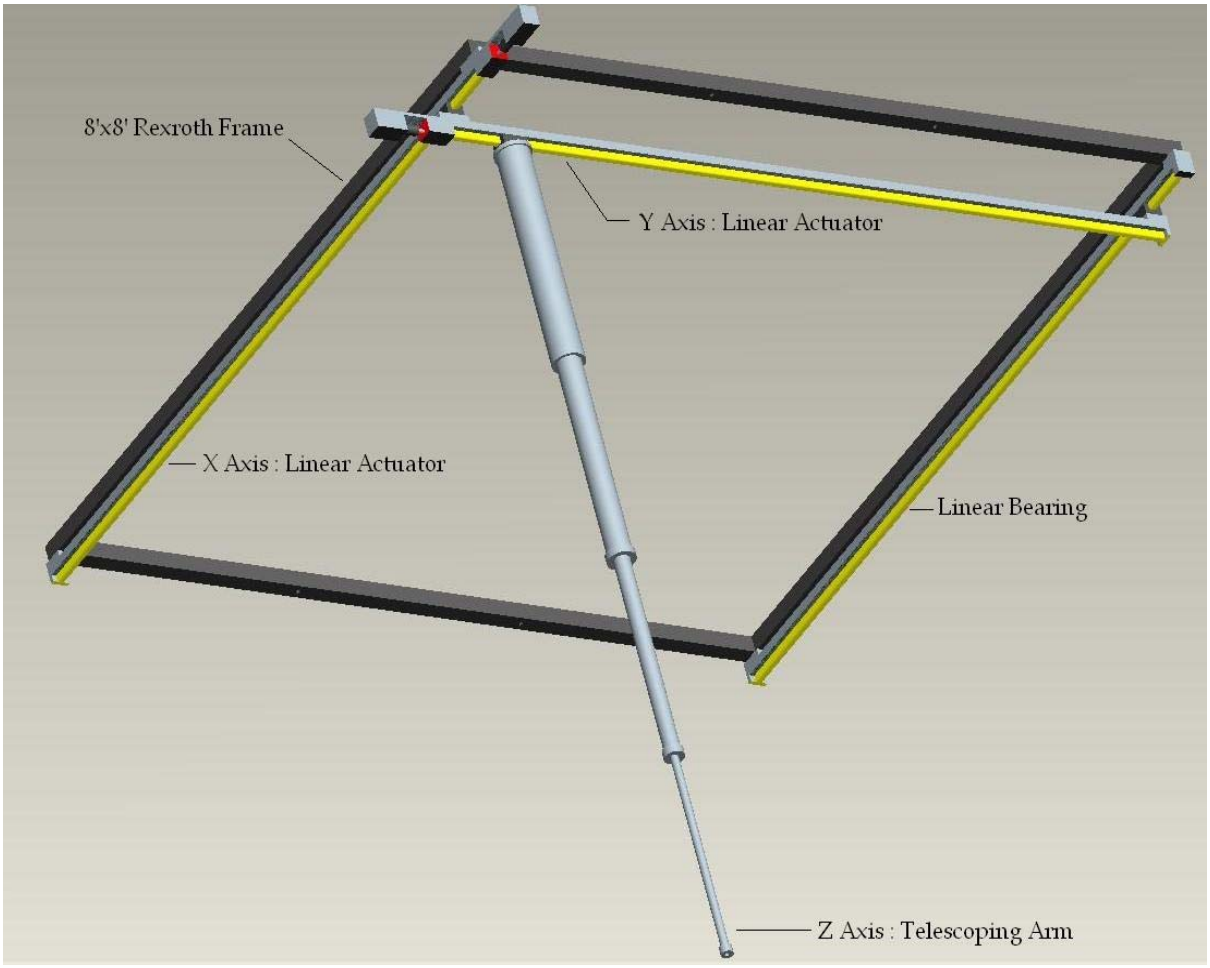

Figure 6.1: Components of the Calibration Device – CAD Model

Each component was decided upon after reviewing many different commercially available products and determining the best choice in regards to compatibility and accuracy as well as price. The attached document titled "Company Contacts" contains the names and contact information for the manufacturers of all components (Appendix B).

6.3.1 Lead Screw Driven Linear Actuators

The lead screw driven linear actuators were purchased from H2W Technologies, shown in Figure 6.2. This company provided multiple revised quotes until a final price and associated hardware design was settled upon, based upon conversations regarding our specific project requirements. A traverse length of eight feet was the maximum standard length available, and this was approved as satisfactory for the ten foot radius range of the transmitter. The device would therefore calibrate one 8'x8' quadrant of the transmitter range at a time, and then be repositioned. This method allows a calibration of approximately 85% of the targeted transmitter area.

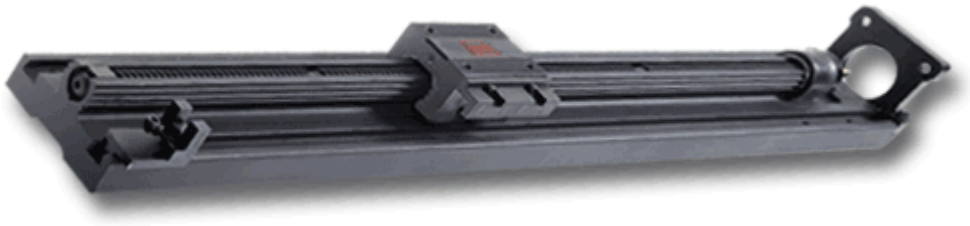

Figure 6.2: Lead-screw Driven Linear Actuator

The rapid guide screw (RGS) is a screw driven linear slide that provides a high linear speed of up to 1.5 meters per second while still yielding very high accuracy over extended travel lengths. The screw has a lead of 0.100" travels per revolution. The manufacturer's stated accuracy along the drive axis is 0.0004 inches/inch, which extrapolates to a maximum error of 0.0384 inches or 0.975 mm over the entire eight foot traverse. This extrapolated accuracy meets the original specification of 1 mm position

accuracy. The stated bi-directional repeatability is 0.000050 inches (50 micro inches), made possibly by the incorporation of an anti-backlash nut design.

The bulk of the RGS (the guide and carriage) is manufactured from extruded aluminum, which is significant because aluminum has a low magnetic permeability. The lead screw is machined from precision rolled stainless steel, which also provides minimal distortion to the magnetic field. The straightness of the travel is established by the guiding outer spline rail. The pitch and yaw axis standards are 0.005 inches/foot and three degrees/foot in the roll axis. Over an eight foot length this later proved to be a problem, considering the accumulated error is an additional 0.04 inches in the pitch and yaw and up to 24 degree in the roll. However, these numbers assume an unsupported rail, and are better any time the rail is mounted to a flat surface (improving pitch and roll) or aligned along a shoulder (improving yaw).

6.3.2 Linear Bearing

A linear bearing and block (rolling mount) was purchased from the company LM76, shown in Figure 6.3. This bearing is economic and works well even if inverted, as is the case in our design, which made it a good choice. Four double angular contacting deep grooved rollers slide with a very low coefficient of friction on RC60 steel shafting. Eccentric inserts on the block provide fine clearance adjustment for various loading. Countersunk mounting holes provide a rigid attachment to the frame every six centimeters. The manufacturer's stated precision for the block surface with respect to the mounting plane is ±0.015 mm.

The linear bearing was required to provide support in the vertical axis for the second cantilevered linear actuator (y axis) being driven by the first actuator (x axis).

Figure 6.3: Linear Bearing

6.3.3Motor Controller

An integrated motor controller was purchased from Optimal Engineering Systems, shown in Figure 6.4. This motor controller integrates the power supplies, controller, micro-stepping drivers, and stepping motors into a single enclosure. It receives commands from the computer via RS-232 serial port communication. The system also can be controlled with a supplied joystick. The joystick provides speed control for all three axes (the knob is twisted for the z axis), where the speed is proportional to the tilt angle of the joystick. The maximum speed for the joystick can be controlled with three

buttons for fast, medium, and slow ranges. The joystick is useful in the fact that the initial position of the calibration device can be easily changed without use of the computer. This allows the device to be set at a convenient location for measuring the receiver's physical position with respect to the transmitter's origin. Once this "home position" is recorded into the software, relative motion can be applied to keep track of the receiver at all times during calibration.

Figure 6.4: OES Motor Controller with Joystick

Each step command sent from the controller corresponds to a 1.8º rotation of the stepper motor. The micro-stepping feature of the motor controller allows up to 256 micro-steps per step, for a total of 51,200 steps per complete revolution.

6.3.4 Telescoping Arm and Drive System

A telescoping arm was machined from nylon stock material. Nylon was chosen as a material to ensure that the arm would not bind while contracting or expanding, because very tight machining tolerances were required to provide accuracy. Smooth motion in the vertical direction was extremely critical for precise positioning of the receiver. Nylon is typically used as a bearing material, due to its low coefficient of friction and high tensile strength. One drawback is it will swell if exposed to moisture, but this was not foreseen as a problem because of the controlled office environment where it would be installed.

Six inch, four inch, three inch, and two inch diameter nylon rods were ordered from McMaster-Carr to provide stock material for the design. Tubes were available from the manufacturer, but they did not have the necessary wall thickness for the application. CAD drawings were created in Pro-Engineer, Figure 6.5, to provide the machine shop at WSU dimensions for each piece.

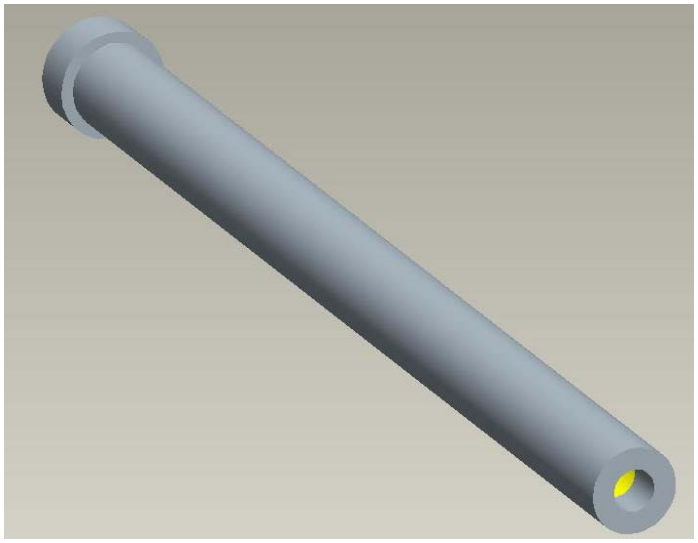

Figure 6.5: Telescoping Design – CAD Model

The rods had to be first drilled and then bored to create a “lip” profile on the inner surface to catch the smaller tube during extension. This required the machining of a custom boring bar, due to the long travel required for the lathe. A typical boring bar is approximately one foot in length, but each tube had to be bored to a length of 2’-9” in order to fully extend to the designated height of 6’-5”, taking overlaps into consideration. Rings were fixed to the bottom of each tube to catch the larger tube during retraction. The travel and overall extended length of the telescoping was restricted due to an I-beam in the ceiling at PACCAR. This beam, which is 127” from the floor, represents the maximum height that a frame can be mounted. As each component of the telescoping arm must retract into the largest diameter tube, the maximum height of the receiver is also limited by the arm’s minimum length. The bird receiver is mounted into a slot fixed to the bottom surface of the telescoping arm. The mounting is aligned parallel to the overhead rails to ensure a zero angle orientation. The completed design is shown below in Figure 6.6.

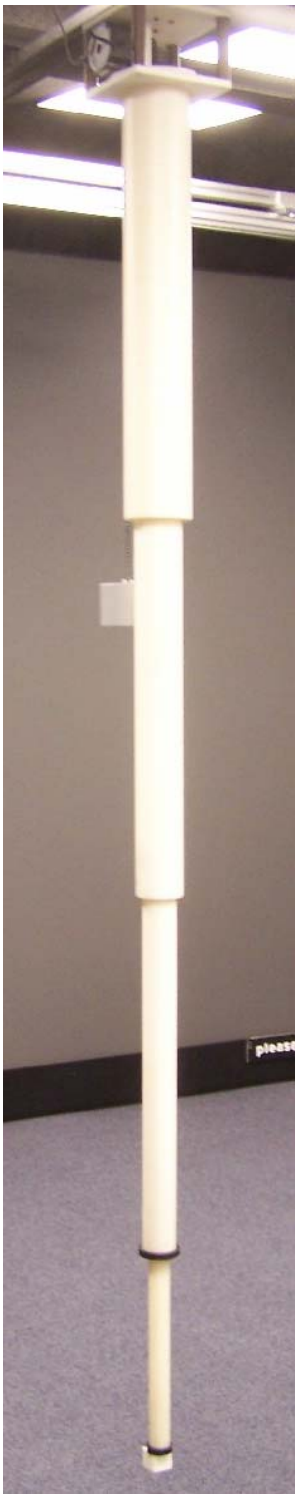

Figure 6.6: Nylon Telescoping Arm

The arm is driven by a NEMA 34 frame stepper motor with a gear sprocket and chain drive system, see Figure 6.7. The chain is made from a high strength plastic; metal

could not be used as it would disrupt the measurements. A mounting plate was hung below the RGS payload that provided enough room for the stepper motor and sprocket to drive the chain system. The accuracy of the drive system is dependent on the pitch diameter of the sprocket as well as the stepper motor resolution:

$$PitchDiameter = 2.550 inches$$
$$Circumference = \pi * P.D. = 8.0113 inches$$
$$BirdTranslation = 8.0113 inches / revolution$$
$$(8.0113 inches / revolution) / (360 \deg rees / revolution) = 0.02225 inches / \deg ree$$
$$(0.02225 inches / \deg ree) / (1.8 \deg rees / step) = 0.04005 inches / step = 1.017 mm / step$$

As the stepper motor driver is capable of 256 micro-steps per step, the telescoping arm drive system therefore has an overall accuracy of 0.003973 mm per micro-step in the vertical axis.

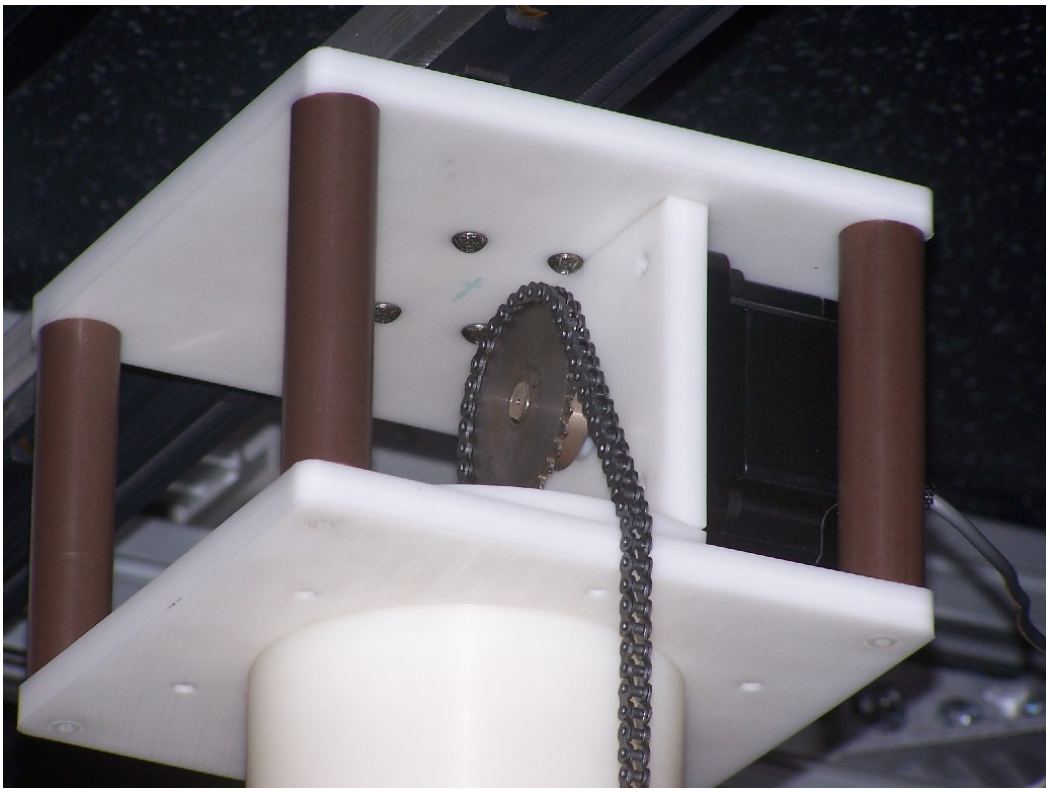

Figure 6.7: Telescoping Arm Drive System

The maximum torque for the NEMA 34 frame motor is specified at 434 ounce-inches. The maximum load is calculated as follows:

$$434 ounce - inches = 27.125 inch - pounds$$
$$Torque = Force * Radius$$
$$Radius = PitchDiameter / 2 = 1.275 inches$$
$$MaximumForce = (27.125 inch - pounds) / 1.275 inches = 21.275 pounds$$

The NEMA 34 motor with a sprocket having a pitch diameter of 2.55 inches is therefore capable of lifting a 21 pound load. We estimated the last three components of our telescoping arm to weight approximately 15 pounds when fully retracted, with the load decreasing as each component is fully extended.

6.3.5 Bosch-Rexroth Frame

The supporting frame system for the automated calibration device was provided by Bosch-Rexroth aluminum extrusion framing. The frame could not be simply welded together, because the entire device had to be first tested at WSU and then dismantled and shipped to PACCAR for final installation. 45x45 mm framing with 10 mm T-slots was selected due to its versatility for connections and accessories, as well as ease of assembly and disassembly. The framing bars arrived in twenty foot lengths, and had to be cut to-length with a cold cut-off saw. Gussets were used to form the right angle connections for the square frame. T-bar, a t-shaped metal bar that can be cut and modified as needed, was used for custom mounting of the components to the framing t-slots.

The entire 8'x8' frame was also mounted to another 16'x8' frame so that the entire device could be moved to calibrate a second quadrant with minimal complications.

Four contact bearings were used to allow the smaller frame to slide along the sixteen foot length of the large frame. The bearings used are EcoSlide carriages, shown in Figure 6.8, also available from Bosch-Rexroth. These carriages, used to mount the smaller frame to the large frame, have Delrin bearing pads that fit inside the framing t-slots to allow motion along the frame. The carriage also has a locking handle to rigidly fix the movable frame during calibration.

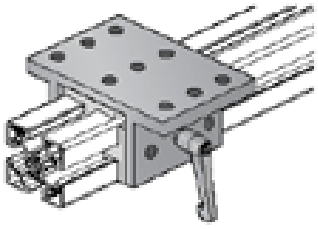

Figure 6.8: EcoSlide Bearing - Drawing

6.4 Assembly and Testing

6.4.1Component Assembly

In order to assemble the components to the frame, various mounting brackets had to be designed. Brackets with through holes along the center line and tapped holes on the edges were machined so that bolts could be screwed up into the framing t-bar while a separate pair could pass through the mounting holes on the RGS linear actuators and screw down into the bracket. The linear bearing already contained mounting through holes along its center line, so t-bar just had to be drilled and tapped for each bolt used to fix the bearing to the frame. To be able to mount the second RGS linear actuator to the

first, we had to drill new through holes in the guide because the existing holes did not line up with the center line for travel in the x direction. These holes were drilled using a milling machine with four decimal digital precision to ensure accurate placing in such an expensive piece of hardware.

6.4.2 Overhead Framing Installation

Once the components for the calibration device were modified and brackets machined, it was ready to be installed for testing. For this to be done, we had to have an overhead frame installed whose height would replicate the environment at the PACCAR site. This frame had to be installed by the WSU Facilities department, which turned out to be a long process involving initial estimates, cost assessments, and finally the actual installation. A square aluminum frame was fixed to the floor as well as hung from the ceiling via I-beam and concrete anchors that allowed us to hang the existing Rexroth frame underneath. The screw stages and the linear bearing were then mounted along with the telescoping arm to begin the testing process.

6.4.3 Testing and Modifications

In order to test the device, we utilized the joystick control mode from the motor controller box. The joystick proved very useful in the testing process, as we were able to move the device in any direction very easily. This mode eliminated the need for any

computer interaction and associated programming, enabling the quick identification of necessary design modifications in the preliminary stages.

Problems arose very quickly after we first put everything together and began running the motors. When we first attempted to raise the telescoping arm the motor began to emit noise at the onset of the additional weight from the third component and would suddenly de-energize, causing the entire arm to collapse violently. I called the manufacturer for the motor controller and the problem was discussed. There was a resistor inside of the motor controller that was restricting the power to the z axis. Once this resistor was replaced the motor was able to receive maximum current and the arm could extend and retract with no problems.

The next problem noticed was that there was quite a bit of lag on the linear bearing while the opposite lead screw was being driven, forcing the assembly to "jerk" forward repeatedly in order to catch up. This was because the lead screw mounted to the frame was on the complete opposite side of the eight foot span from the linear bearing, and the long distance compounded the small amount of friction present in the bearing. To fix this problem, we ordered a second bearing rail and block and moved the lead screw to the middle. With the drive system in the middle it eliminated any uneven motion parallel to the direction of travel.

The second problem encountered was that the telescoping arm would tend to rotate unpredictably about its axis during extension and retraction. This problem was unacceptable because the algorithm is assuming a zero angle orientation at all times. We spoke with the machinists and decided to put keys and slots in each section, Figure 6.9, which would force the pieces to stay aligned with the drive chain. The key is simply a

nylon screw that had the threads removed from the tip. This created a cylindrical extrusion that when set at the proper depth keeps the slot in the next smallest tube aligned properly. This solution worked very well and the telescoping arm operates as originally designed.

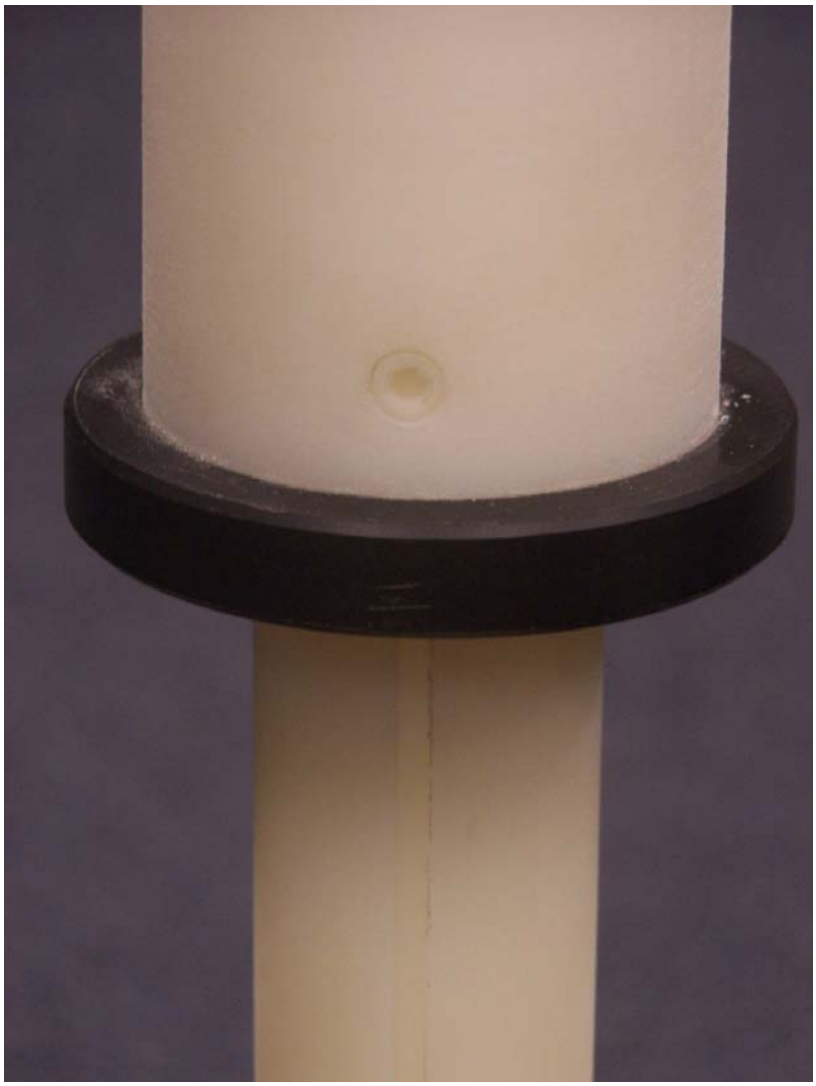

Figure 6.9: Key and Slot Alignment

6.4.4 Completed Assembly

The fully assembled and installed calibration device is shown below in Figure 6.10:

Figure 6.10: Calibration Device Installed

7. Integration with COVE

7.1 Overview

In order to fully automate the calibration process, the device had to be run completely by the COVE software. This involved integrating stepper motor commands into the data collection process to position the receiver at each user-specified grid point. This method would eliminate the need for a time-intensive calibration, allowing the engineer to collect as many data points as necessary without requiring a time-accuracy tradeoff.

7.2 Existing COVE Capabilities

When COVE is executed, the user has the option to either create a new space or open an existing file. The space contains the minimum and maximum x, y, and z values that specify the physical range of the volume to be calibrated, as well as the increment in each direction (Figure 7.1).

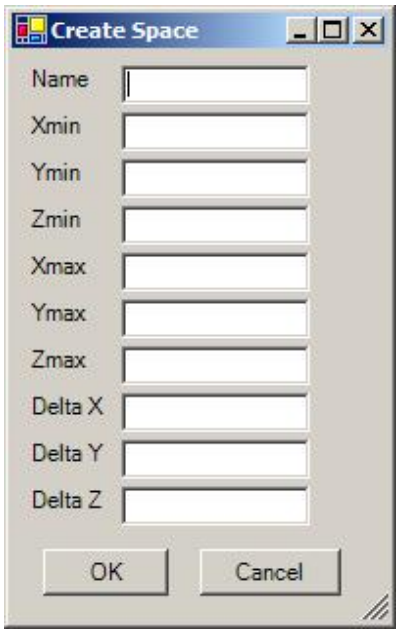

Figure 7.1: Creating a Space

Once a space has been created, it can be saved on the hard drive into an XML file format. A calibration space can contain any number of regions, with every space having a minimum of one region. This allows the user the option of designating sub-regions with varying densities, allowing a fine calibration for given areas of interest inside of the calibration space. Upon creating of a space and its associated regions, an OpenGL display (implemented by Youngjun Kim) shows a representation of the grid points (Figure 7.2). This display shows the current selected region in red, while other sub-regions are displayed in yellow.

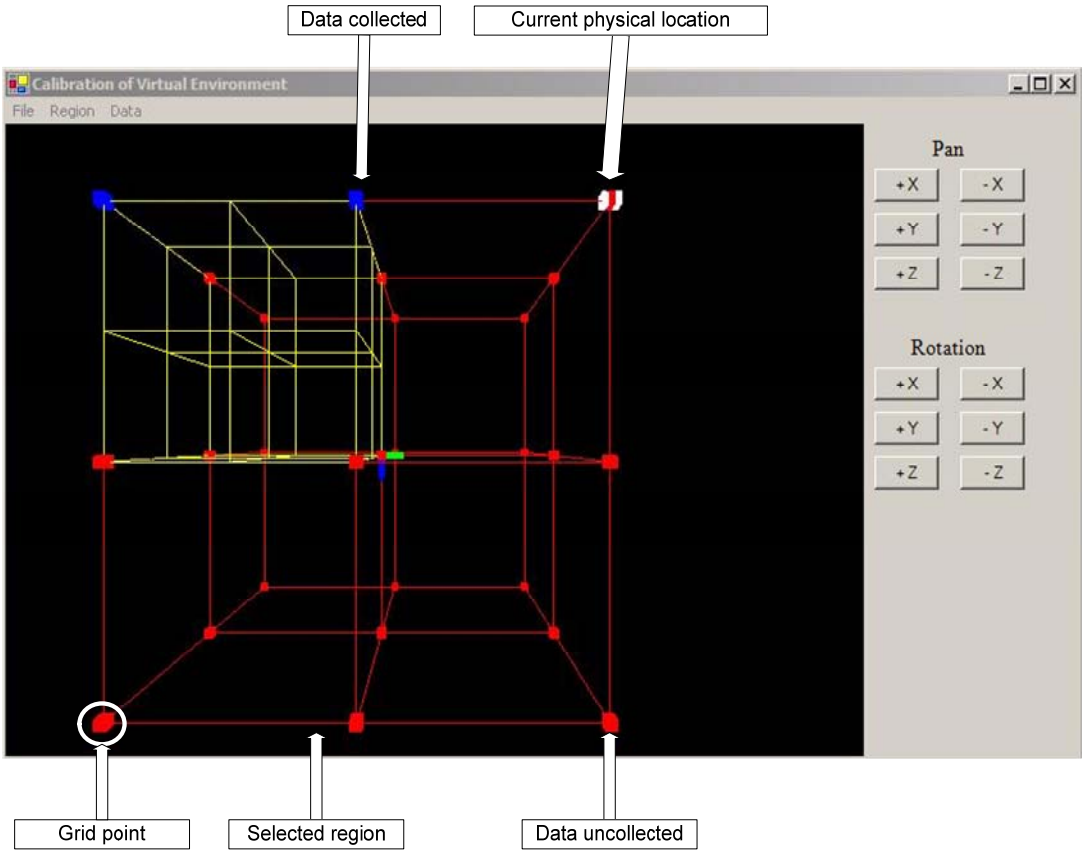

Figure 7.2: Sample Calibration Space and Region

Once the user has a region set up, they can choose to collect data from the Data menu. This option brings up a selection window that asks which particular region in the calibration space is to be calibrated. Once a region is selected the collect data window form is opened. This form is for collecting the data from the tracking device. The capabilities of this form are as follows (Figure 7.3):

- Connect to the server where the tracking device runs.
- Show the physical position of the receiver.
- Show the collected data from the tracking device.

- Show the current tracking device data.
- Show the number of collected grid points out of the total number.

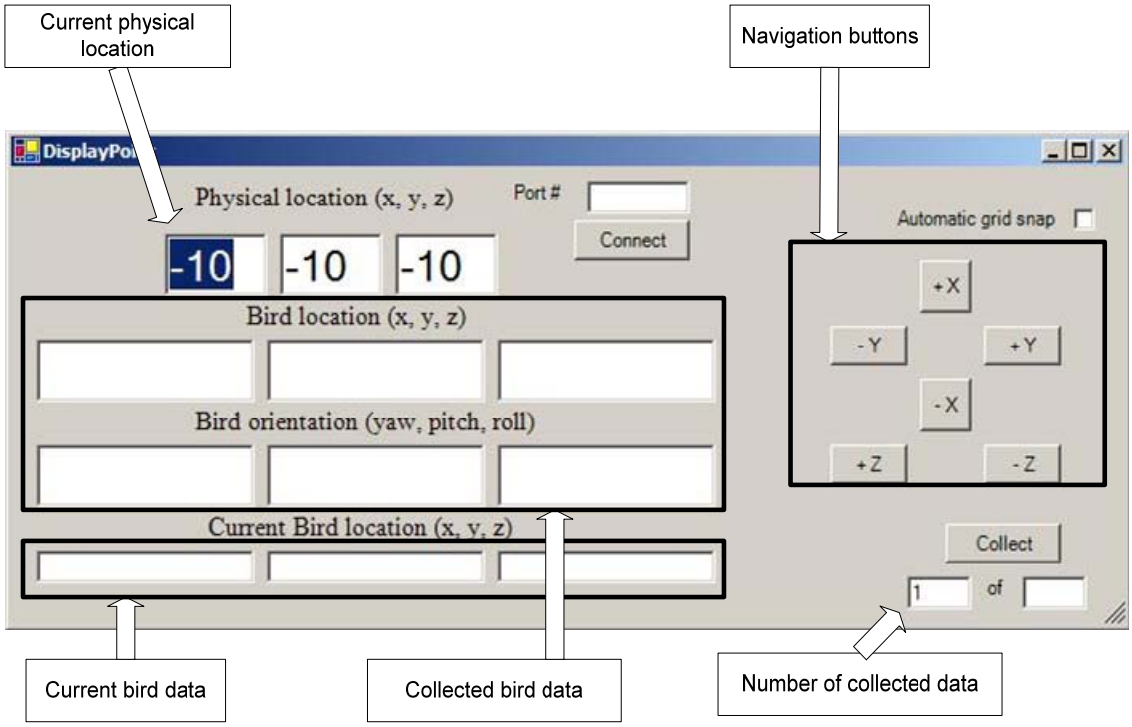

Figure 7.3: Data Collection Form

If you click one of the navigation buttons, this form will update the current physical position. In addition, a green cube will show the current location in the main GUI. Therefore, in order to collect data the user must step through each grid point using the navigation buttons, while simultaneously moving the receiver to the reported physical position, until the entire region has been calibrated. Collected grid points are displayed using a blue cube, while points still to be collected are displayed as a red cube. This color scheme ensures that all of the points are calibrated during the manual process, the user is free to pan and rotate in x, y, or z inside the graphical calibration space for verification of a complete data set.

7.3 COVE Automation Modifications

In order to automate the data collection process modifications were made to the existing C/C++ code. The goal was to eliminate the manual selection of the grid points, in favor of an automatic cycle through every point. At each step in the cycle, commands were to be sent to the stepper motors to place the receiver at the current physical location for the grid point.

The OES motor controller communicates with the computer via RS 232 serial port. In order to provide commands from the C/C++ code, a software package was purchased from MarshallSoft Computing titled "Windows Standard Serial Communications Library". This library provides calls to the Windows serial port API, and was used to allow function calls for:

- Opening the serial port for communication.
- Receiving the current location of each motor.
- Setting movement parameters for each motor.
- Communicating when a motor had completed its movement.

When a call is sent to the motor controller it must receive acceleration, velocity, and final location. The final location can either be an absolute or relative distance. Our program utilizes completely absolute distances to provide an absolute reference frame for the receiver at all times. To accomplish this, a "home position" must first be set at the beginning of the program execution. This home position represents the physical location

of the receiver with respect to the transmitter before calibration begins, the home position can be chosen with the joystick for ease in measurement. Every movement is then calculated with reference to this home position to determine the correct rotations. A conversion is required from translation in inches to rotation in micro steps:

$$Rotation = Translation * 256(microsteps / step) * 200(steps / revolution) * 10(revolutions / inch)$$

This example is for the RGS linear actuator, where a 0.1" lead requires ten revolutions to translate one inch.

The algorithm for the automated movement is designed to provide efficient use of time, eliminating unnecessary movement during calibration. A flow chart for this process is detailed in Figure 7.4. To accomplish this, the data points are traversed in an alternating format. The very first movement command given to the motor is to move from the current home position to the maximum x and y values and the minimum z value. The minimum z value is actually above the transmitter, as the tracker coordinate system has a positive z direction towards the floor. From this retracted position of the telescoping arm, the algorithm will step through each grid point along the z axis (extending the arm) until the lowest grid point is reached. Next, the y axis lead screw is commanded to translate to the adjacent grid point and the data points are collected in the reverse order until the highest grid point is reached (retracting the arm). The same methodology is used for the x and y movements, utilizing a sign change to eliminate unnecessary movement.

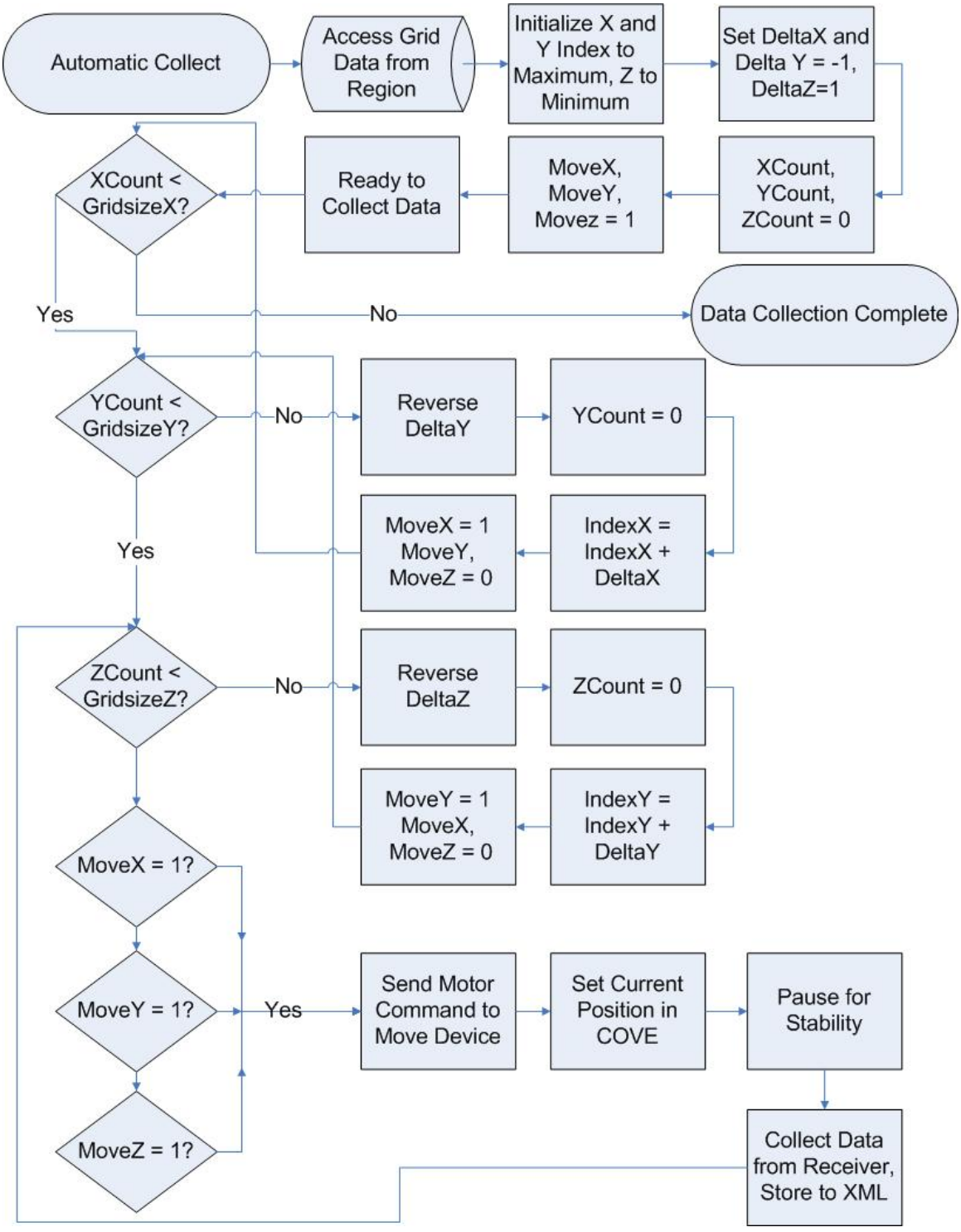

Figure 7.4: Automated Movement Flowchart

Buttons were added to the collect data windows form in order to automate the data collection process, shown in Figure 7.5. The user must first select a serial port number where the motor controller is connected to open the port for communication. Next, they must measure the initial position of the receiver with respect to the transmitter and enter this into the home position. Once this has been completed, selecting the Automatic Collect button will cause the calibration device to move to the first grid point and begin the data collection process. No further input is required, as the algorithm steps through every grid location and moves the receiver to the corresponding physical location. Upon completion the data for the physical location as well as the associated tracker readings are saved into the XML region file.

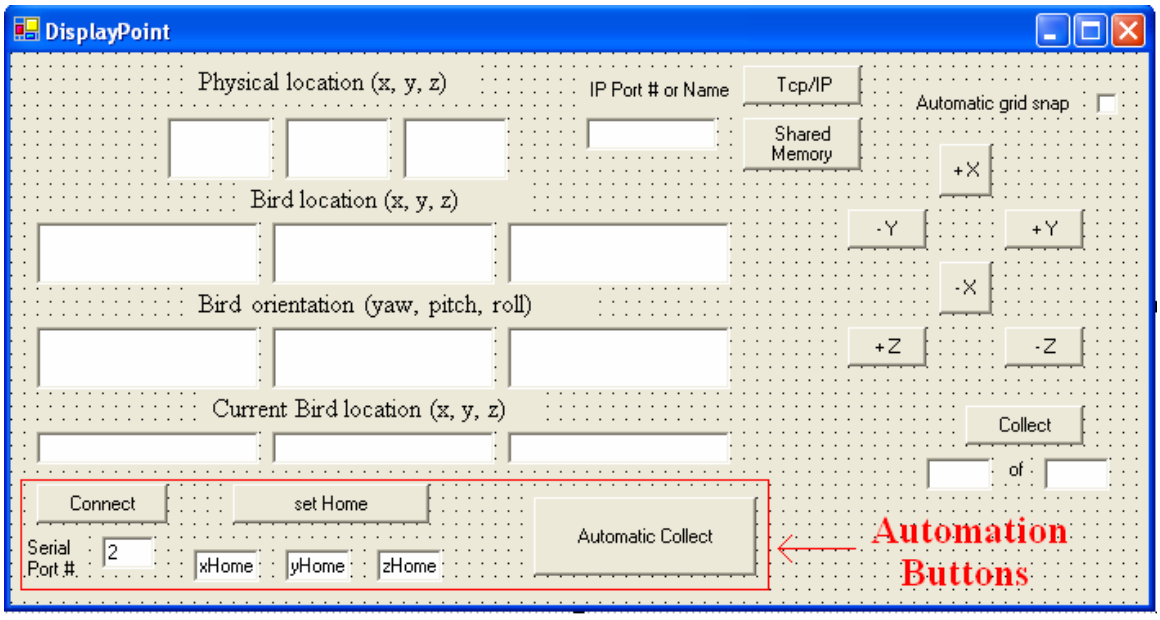

Figure 7.5: Automated Data Collection Form

8. Implementation of Collision Avoidance

8.1 Overview

The final phase of the project was to implement collision avoidance during the collection of data. The goal was to have the calibration device avoid static, or stationary, objects inside of the tracking space. This would allow the calibration of a tracking environment containing commonly occurring obstacles such as a chair or steering wheel for engineering simulations in VR.

8.2 Collision Avoidance Algorithms

Collision avoidance is a very common problem for robotics applications. Collision avoidance algorithms can be divided into two categories: global and local. Global methods assume a complete model of the robot's environment is available before run-time. This allows an "offline" calculation of a target path, eliminating the need for additional movement planning during operation. Local or reactive methods use only a small fraction of the world model to calculate an avoidance path. Local methods utilize sensor input to constantly determine their proximity with respect to the surroundings.

It was decided to utilize a global method for collision detection of the automated calibration device. This was because the addition of sensors on the robot arm would generate noise and interfere with the tracker readings, reducing the accuracy of the results.

The global method is possible because all of the obstructions in the environment are stationary and collision regions can be identified before the data collection process. From the collision regions a movement path can be calculated to position the receiver at each possible grid point.

In identifying possible collisions, a method must be developed to calculate the minimum distance between the robot and obstructions, see Figure 8.2.

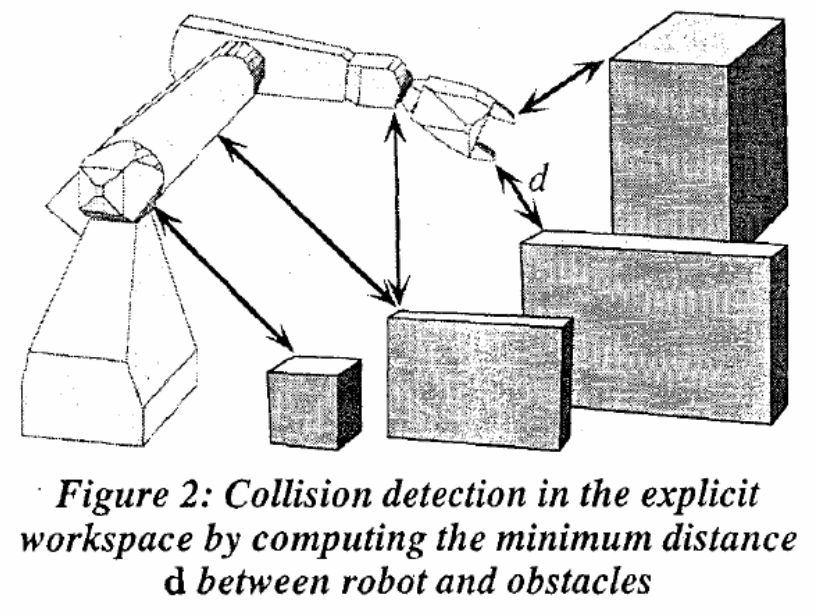

Figure 2: Collision detection in the explicit workspace by computing the minimum distance **d** *between robot and obstacles*

Figure 8.1: Minimum Distance Computation [17]

To calculate this distance, one must have a methodology for representing the geometry for every object in the environment. This geometry representation will be specific to the application, and can vary from an exact model of the robot and obstacles to a simple bounding box for very rough calculations. A diagram of the various representations appears below in Figure 8.2:

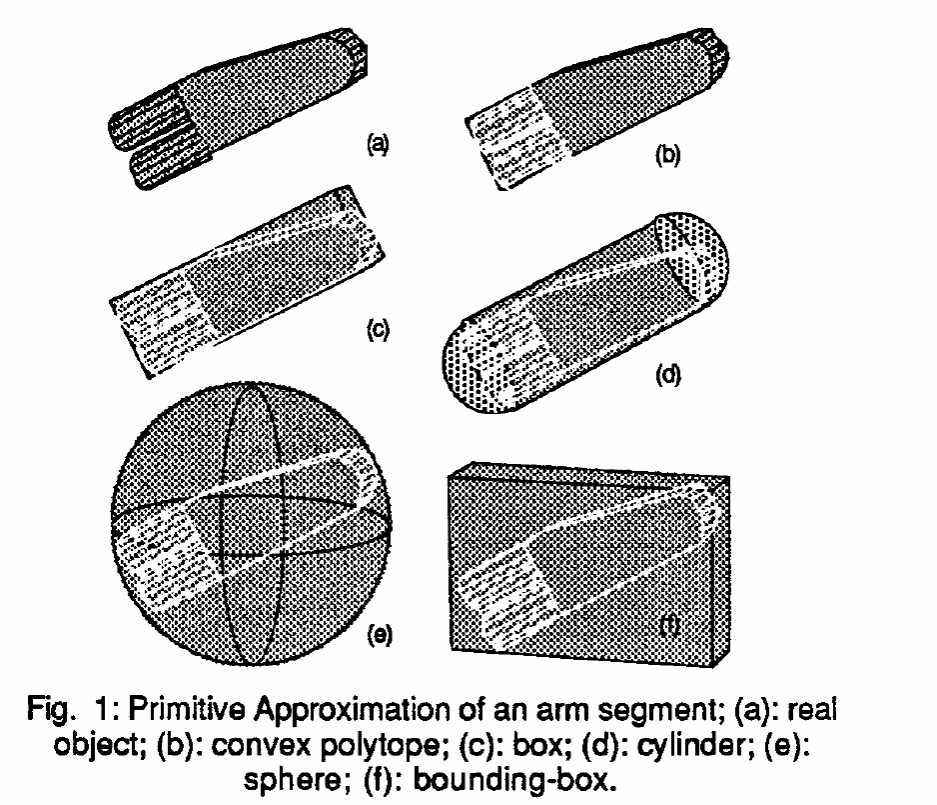

Fig. 1: Primitive Approximation of an arm segment; (a): real object; (b): convex polytope; (c): box; (d): cylinder; (e): sphere; (f): bounding-box.

Figure 8.2: Geometric Representation [17]

The complexity of the model for geometric representation will have a direct effect on the difficulty and associated computational time of the minimum distance calculation. Very complex methods are required for calculating the distance between complex surfaces, whereas an extremely simple equation is required for intersections between bounding boxes.

8.3 Methods Considered for Collision Detection

One idea for the global collision detection method was to represent all objects in the environment by a collection of small cubes, or voxels. An example of a voxel representation for a sphere is shown in Figure 8.3.

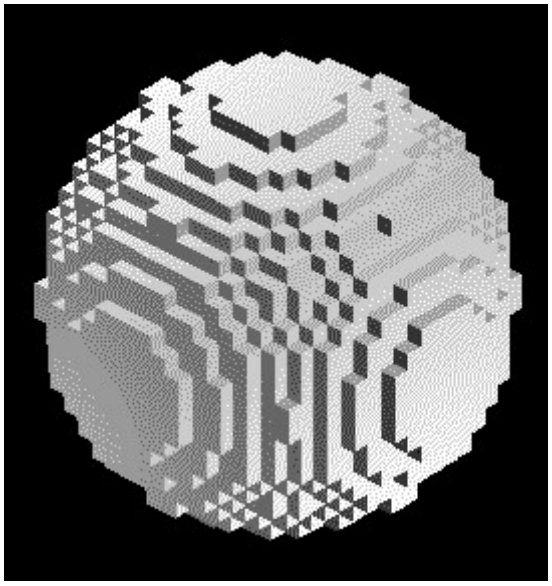

Figure 8.3: Voxel Representation

By decomposing the three dimensional volume into voxels, every location could be identified as either occupied or empty. The advantages of this method would be its simplicity and ease of programming. The disadvantage would be its inaccurate representation of complex objects for collision detection, to implement this representation the voxel size would have to be fairly large for practicality in the modeling phase.

The idea chosen for the collision detection algorithm was to generate a two dimensional array of height values for a discrete region based on the calibration resolution. This algorithm is very similar to a Z-buffering in computer graphics. A Z-buffer stores depth values to determine which elements in a three dimensional environment will be displayed on a two dimensional screen. The buffer is arranged as a two dimensioned array (x, y) of depth values, with one element for each screen pixel. If another element in the scene must be rendered in the same pixel, the graphics card compares the two depths and chooses the one closer to the observer. The chosen depth is

then saved to the z-buffer, replacing the old one [18]. In this particular case, the size of the buffer is based on the resolution of the grid points specified in COVE by the user. The depth values come from a CAD model, with the surface represented by a triangle mesh. The algorithm indexes through all of the triangles to determine the tallest and stores its height value for each grid point at the current (x, y) location. The advantage of this algorithm is that it can be used to represent very complex objects to avoid in the motion planning stage, with the accuracy of the collisions defined by the accuracy of the triangular surface mesh. The CAD model can also be easily updated and the depth values recalculated to account for configuration changes of objects in the tracking environment, requiring only one computation time per configuration.

Figure 8.4 is a representation of the maximum height calculation for a very basic CAD model. A chair is modeled in the room, using the origin of the transmitter as a reference point. It is important that the origin of the transmitter coincides with the coordinate system of the CAD model to ensure that the calculations are performed correctly. Yellow cylinders display the maximum height that the telescoping arm may descend at each grid point based on the collision detection algorithm. The grid from the region is displayed on the floor, showing the (x, y) locations at which the calibration device will collect data. The maximum obstruction height was calculated from the IV model at each grid point, if no obstruction is calculated the maximum height is equal to the lowest grid point for the region. While this example is relatively basic, the algorithm will work with very complex models as well as any desired grid spacing for the calibration data.

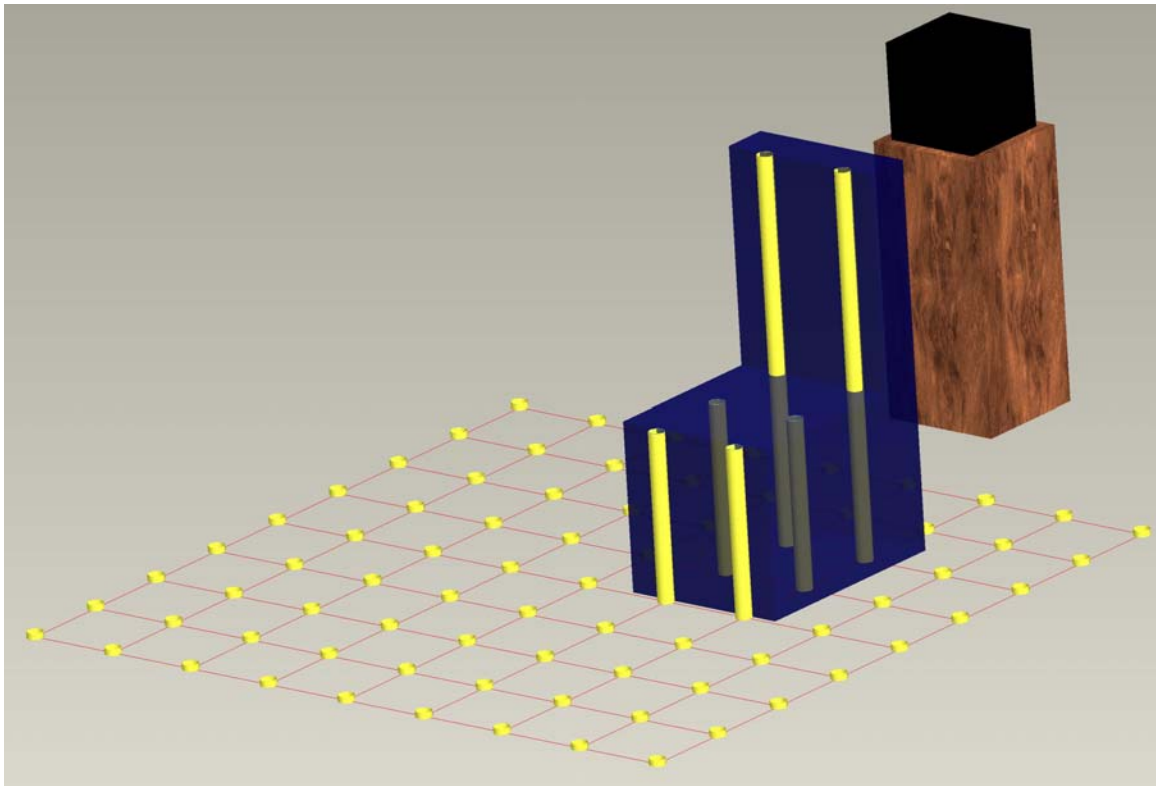

Figure 8.4: CAD Collision Detection

8.4 Collision Avoidance Implementation

To implement the collision avoidance algorithm, simple test-case models were created in Pro-Engineer. These test case models contained simple rectangular obstructions and were used to verify the validity of the program. These CAD model were then saved into an Inventor (IV) file format. An Inventor file represent a complex surface as a triangular mesh (Figure 8.5); it contains both a set of triangle normal vectors and (x, y, z) position data for each triangle of every component in the assembly.

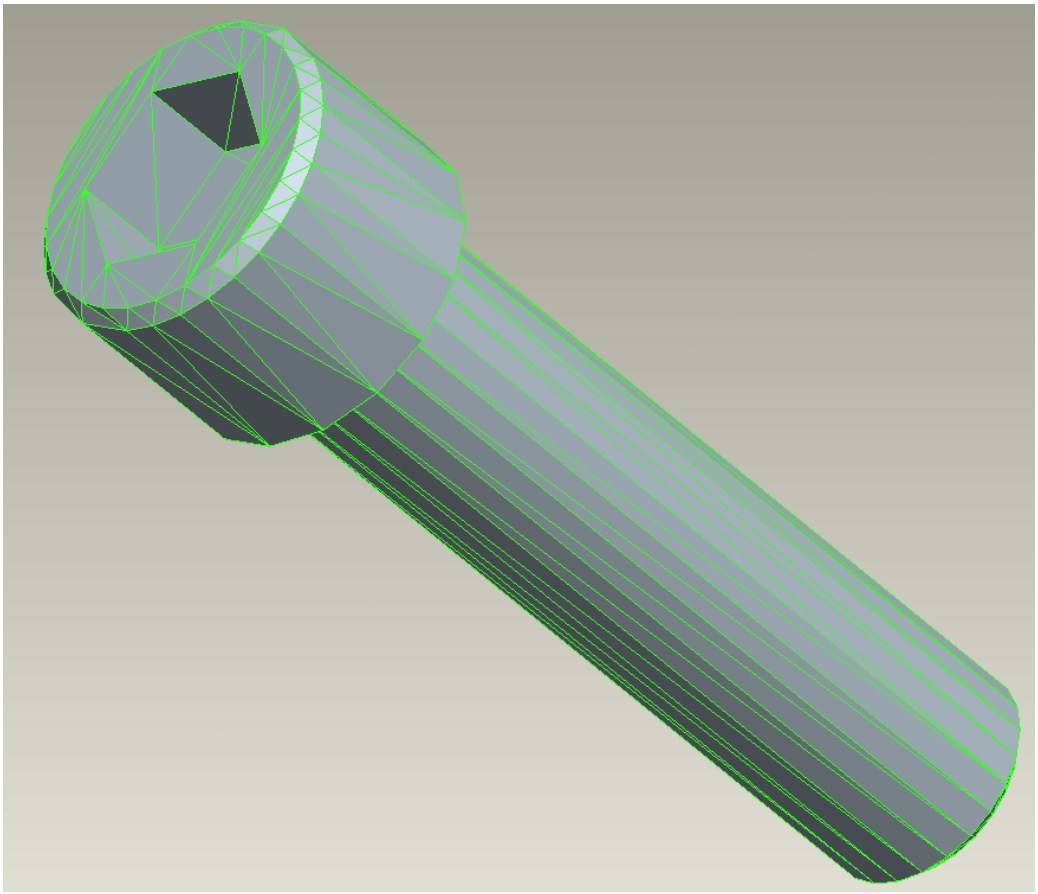

Figure 8.5: Triangular Mesh of a CAD Model

Code was incorporated into the C/C++ COVE software to load the IV file data into memory. The algorithm to determine the maximum height values for each grid point is detailed in a flow chart, Figure 8.6. First, the number of polygons is determined, and from this an array can be dynamically created to store the location of each vertex of the triangles. A separate array is dynamically allocated to store the maximum height values based on the resolution of the grid points in the X, Y, and Z directions. This dynamic array is initialized to contain a default maximum height of -999 at each location. Next, every triangle vertex in the array is parsed to calculate if it is within a specified tolerance of each grid point. The tolerance is variable according to the height location corresponding to the changing diameter of the telescoping arm. The algorithm then uses

the Z-buffer sort, if the triangle vertex is located within the tolerance of a grid point the Z value is checked against a stored maximum height for that particular (x, y) location. If the z value is greater, it then becomes the maximum height for that particular location. This effectively creates a two dimensional maximum height histogram, storing the maximum height for every grid point in the specified calibration region.

In order to avoid collisions with the objects, a check is incorporated into the automatic data collection process in COVE. At every location, the next Z value is compared with the maximum height for the current (x, y) location. If the value is less than the maximum height, the telescoping arm is directed to retract fully to the top of the calibration region and proceed to the next grid point. This algorithm also requires that if the device is at the end of a particular X or Y traverse, it must check the next grid point to determine if a collision will occur. If a collision is calculated the arm will also retract to the top and continue the cycle. Data points that are constrained by collisions are thus simply not collected, and marked as such in the program.

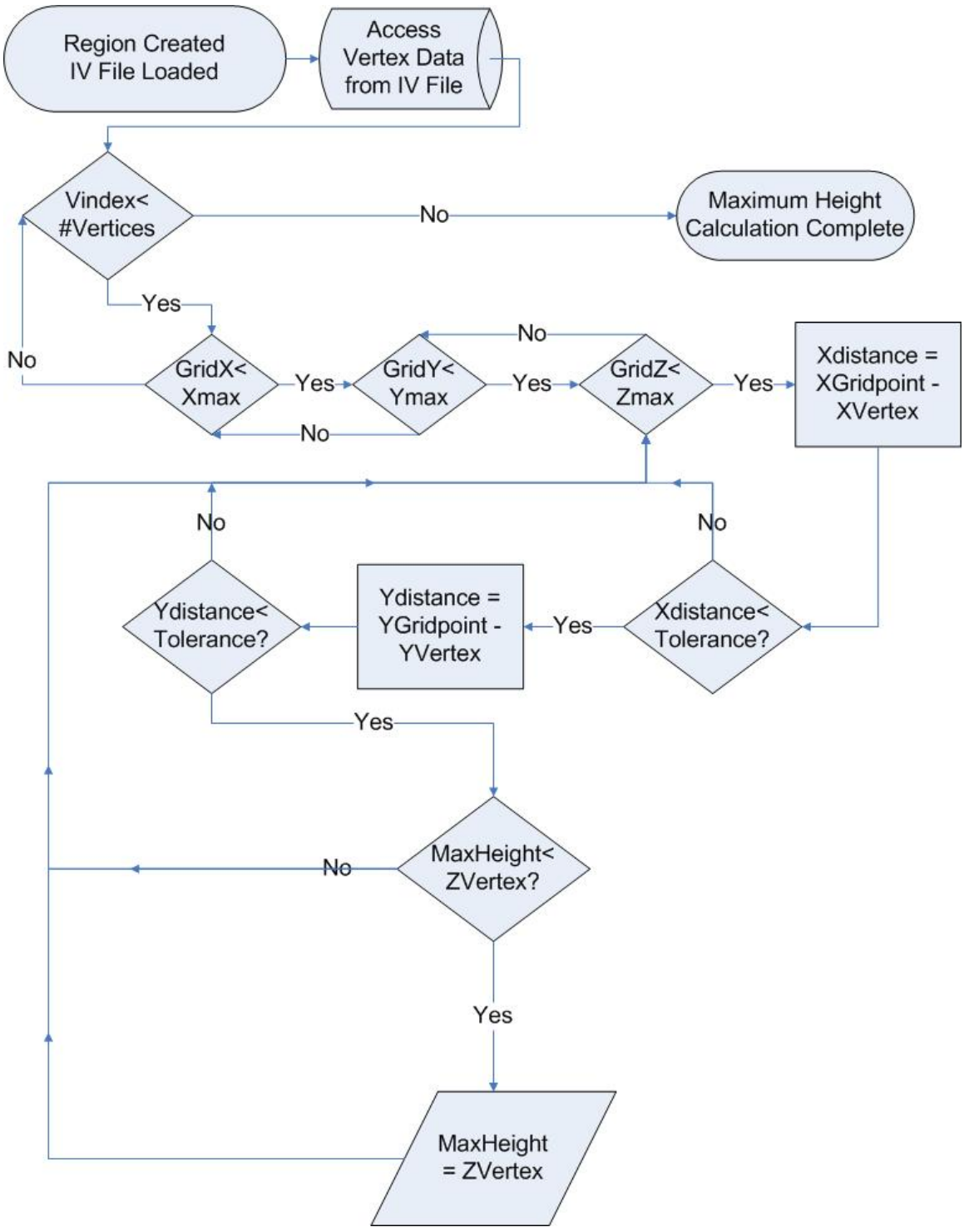

Figure 8.6: Maximum Height Calculation Flowchart

9. Calibration Data

9.1 Calibration Procedure

The calibration device was used to conduct a full calibration of an 8’x8’x6’ volume. The grid points were selected such that the receiver was always at a minimum of two feet from the transmitter. This minimum distance is necessary because data collected too close to the transmitter is unusable due to magnetic saturation. A CAD model of the room was created containing the walls, floor, and transmitter as well as a truck seat commonly used for engineering simulations. The truck seat was included to demonstrate the collision avoidance algorithm. This CAD model was converted to an IV file and loaded into COVE to calculate possible collisions.

Before calibration can begin, the obstructions must be positioned with respect to the transmitter based on the CAD model dimensions. In order to accurately position the truck seat an AccuLine Pro laser level was used to ensure that the measured surfaces were parallel to the receiver, Figure 9.1. The laser level projects a straight line perpendicular to the base, which is leveled using the incorporated bubbles, onto any surface. The level was also used to precisely calculate the Cartesian “home” position of the bird with respect to the transmitter. The positional accuracy using a tape measure and laser level is approximately ¼”.

Figure 9.1: Laser Level for Position Measurements

The accuracy of the home position is crucial because it is input into the COVE software before calibration begins, and is used as a reference for further movement to each grid point. Any error in the home position decreases the physical accuracy for the positioning of the receiver at each grid point. An inaccurate home position will cause a poor correlation to physical objects in the environment, such as a truck seat for ergonomics applications, but will not adversely affect the accuracy of virtual objects. Virtual accuracy is considered to be a relative accuracy inside of the virtual environment, and has no association with the actual physical position.

The data points were collect in 12” intervals in the x, y, and z directions inside of the 8’x8’x6’ region. The region was roughly two feet in front of the transmitter in the X direction, centered about the origin of the transmitter in the Y direction, and extended from just above the floor to a maximum grid height of six feet in the Z direction. The lowest Z value was measured to be ¾” from the floor, or 39.25” below the transmitter origin. The x values started at 25.5” in front of the transmitter and progressed to a distance of 121.5”. The y values began at 45.5” to the left of the transmitter (facing the screen) and ended at 50.5” to the right. This grid density required the acquisition of 384 data points.

24 grid points were bypassed and data at these locations was not collected due to collisions detected with the truck seat. At each grid point, the software checked to see if the next point was constrained due to collision with an obstruction (the truck seat in this case). The telescoping arm started at each (x, y) location in the fully retracted position, it would then descend in one foot intervals to collect data. When the arm was positioned above the seat, it descended to the last grid point above the obstruction and then retracted back up to the maximum grid height for movement to the next y position, Figure 9.2.

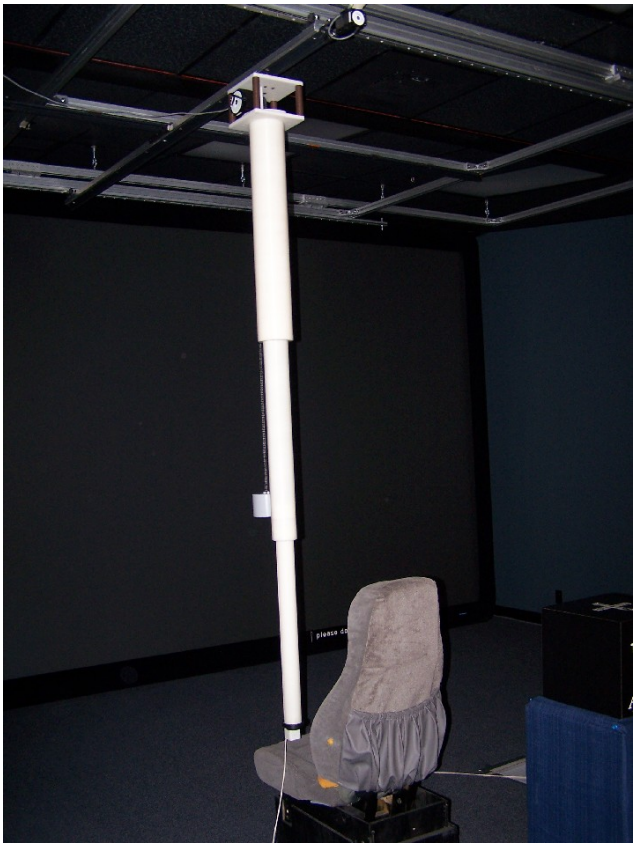

Figure 9.2: Calibrating Around Obstructions

Interaction with the engineer for the calibration process takes approximately five minutes to set up a region, load an IV file, calculate collisions, and connect to the motor controller to start the automated data collection. The calibration took 2 hours and 49

minutes to complete, noting that the entire process was automated and required no intervention from the user beyond the initial setup time. This time was mostly restricted by the telescoping arm which required approximately two minutes for descending to each of the six grid points, waiting long enough to record the data from the receiver, and then proceeding. At the lowest grid point for every (x, y) location the arm would retract to the highest grid point at 32.75" above the transmitter origin. Next, the y axis would move and take approximately 30 seconds to traverse to the next grid point. At the end of each y-z plane the x axis would also take 30 seconds to traverse to the next grid point.

9.2 Data Analysis

9.2.1 Data Management

The data set from the completed calibration is saved into an XML format by the COVE software. An example of an XML file is show in Figure 9.3, each grid point contains:

- The current index of the 9x9x7 array.
- The (x, y, z) coordinates for the physical location of the receiver.
- The (x, y, z) coordinates from the receiver.
- The (yaw, pitch, roll) from the receiver.
- YES or NO - if the data point was collected or skipped due to collision.

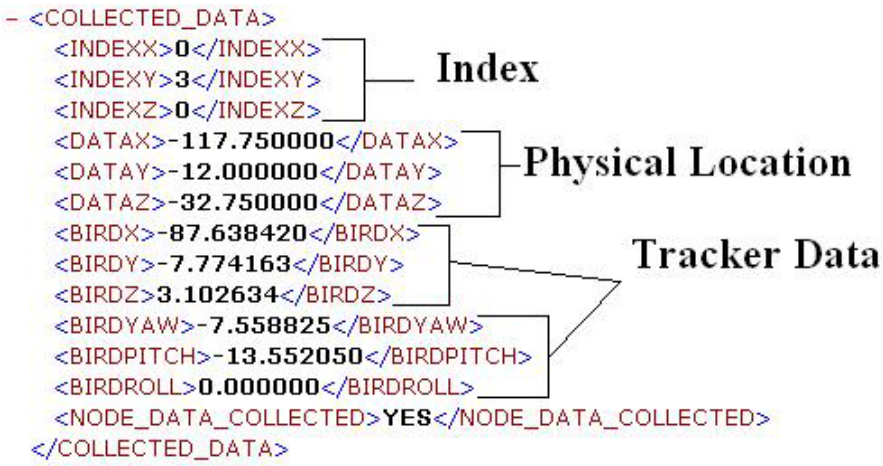

Figure 9.3: XML File

To analyze the data, the XML file was imported into EXCEL. The error was computed for each component axis as well as overall the combined root mean square error.

9.2.2 X Component Error

The error in the x component fit the expected trends, error increased as distance from the transmitter increases. This effect is not linear because surrounding distortion is magnified as the distance increases and the magnetic field strength is weakened. Error was measured as the absolute difference between the reported receiver information and the true physical location. The x component was averaged across the entire y-z plane to get a single value for each of the 8 distances in the x direction, Figure 9.4.

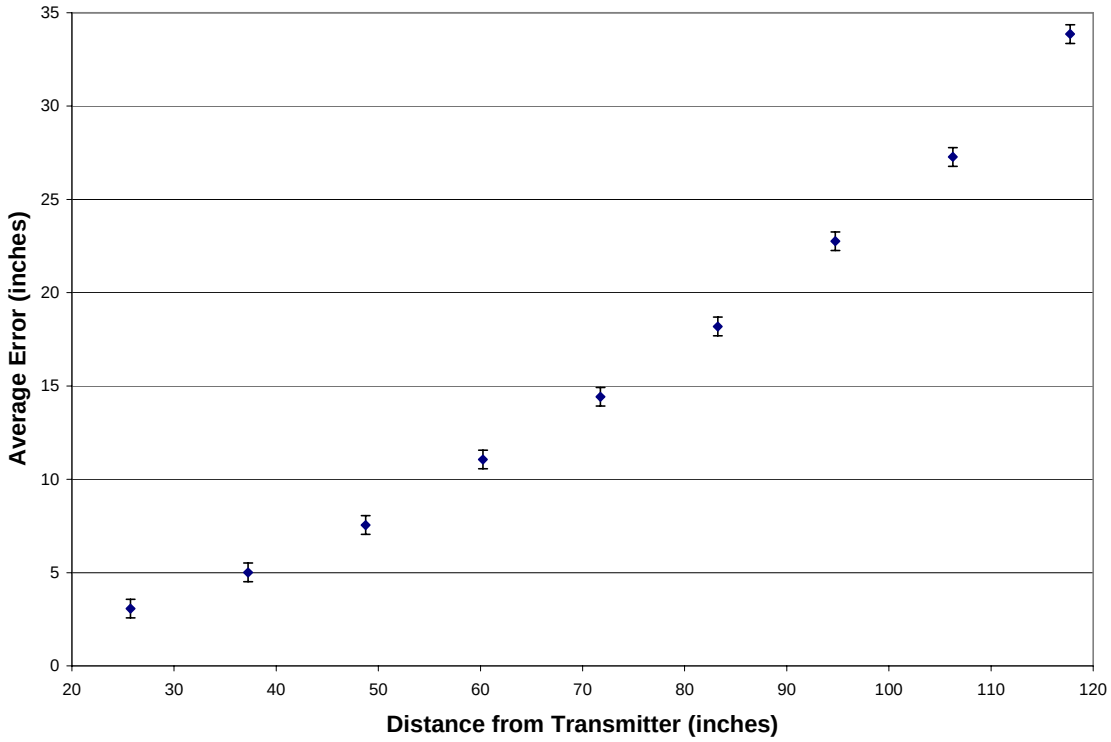

Figure 9.4: Error in the X Component

9.2.3 Y Component Error

The error in the y component is much different than the other two axes. It has no particular trend but instead appears to be sporadic, see Figure 9.5. This unpredictable error is due to the effect of the massive steel I-beams in the floor and ceiling structures of the PACCAR lab. While this metallic distortion has an effect on all of the components, it is much greater for the y axis. This is because the orientations of the beams are parallel to the y axis; large metallic objects parallel to a measurement axis magnify the distortion greatly [6].

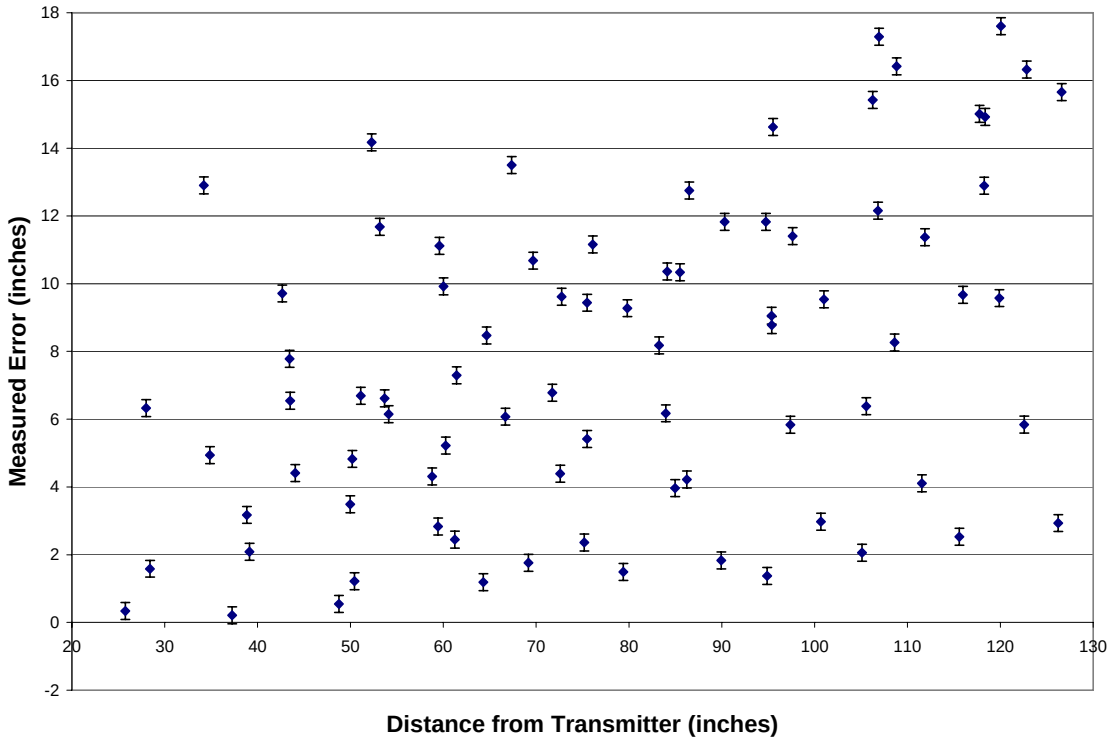

Figure 9.5: Error in the Y Component

9.2.4 Z Component Error

The error in the z component also behaves according to the expected trends: error greatly increases as distance from the transmitter is increased, see Figure 9.6. The absolute error from the 6 values for the z component was averaged at every (x, y) location. The six components were averaged because the point closest to the floor was consistently much more distorted due its proximity to the metallic objects in the floor. Plotting each individual error value yielded no discernible trend because of this. The distance from the transmitter for the averaged error value was approximated as the hypotenuse of the x and y distance.

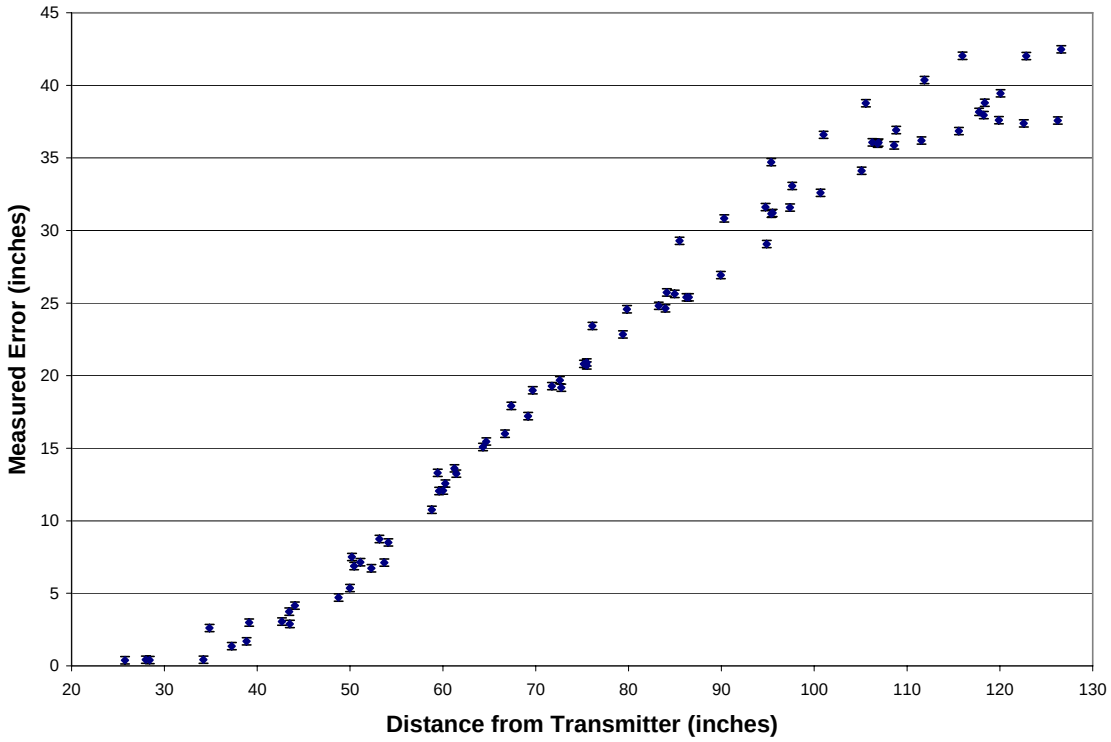

Figure 9.6: Error in the Z Component

9.2.5 Root Mean Square Error

The error components at each location were also combined to calculate the root mean square error. The root mean square (RMS) is defined as:

$$RMS = \sqrt{\frac{X\_error^2 + Y\_error^2 + Z\_error^2}{3}}$$

The RMS is plotted as a function of distance from the transmitter and appears below in Figure 9.7.

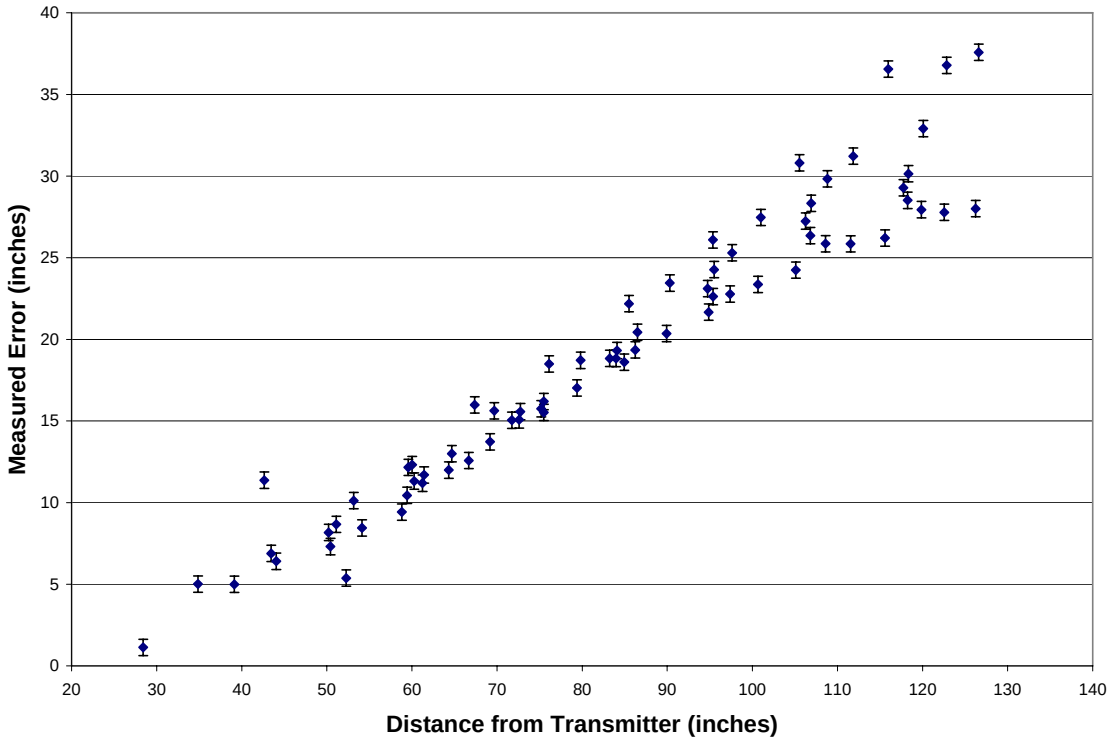

Figure 9.7: Root Mean Square Error

This plot once again shows that error increases greatly as distance from the transmitter increases. It is, however, hard to use this two-dimensional graph in order to obtain a meaningful understanding of the error field present in the tracking environment.

9.2.6 Error Visualization

Utilizing a three dimensional format provides a much better tool for representing the magnetic error present in a tracking volume. In order to accomplish this, it was decided to use curve fitting to plot an "error surface" of the RMS error at each grid point's (x, y) location. This plot can be generated for each z value to get a full range of surfaces representing the error at every collected grid point in the environment.

Commonly available curve fitting methods will not represent the error in an acceptable method for analysis due to the unpredictable changes in the data. Therefore, it was decided to use Bezier curves to interpolate the data points. In order to accomplish this, an inverse design algorithm is necessary to calculate the control points of the curve. These control points are then used to plot a Bezier curve that is forced to interpolate every collected data point.

To represent the error surface, Bezier curves were plotted in two directions. The RMS error was fitted to a curve in the Y direction, with nine curves corresponding to the nine different X locations. Next, the RMS error was fitted to a curve in the X direction and repeated for each of the nine Y locations. The resulting surface for a Z value of 32.75 inches above the transmitter appears in Figure 9.8 This graph is very effective at visualizing the error trends experienced by the electromagnetic tracking system. As one can see, the error is the lowest closest to the transmitter at a value of Y = 0 and X = -25.75 inches. From there, it curves upward to the right and left of the transmitter as the distance increases in the Y direction. As the X direction also increases so does the error. In particular it can be noticed that the error surface greatly lifts towards the rear-left of the transmitter. This is due to the presence of metallic beams in the wall, with their distortion effect being magnified by the decreasing signal strength from the transmitter at such a long range.

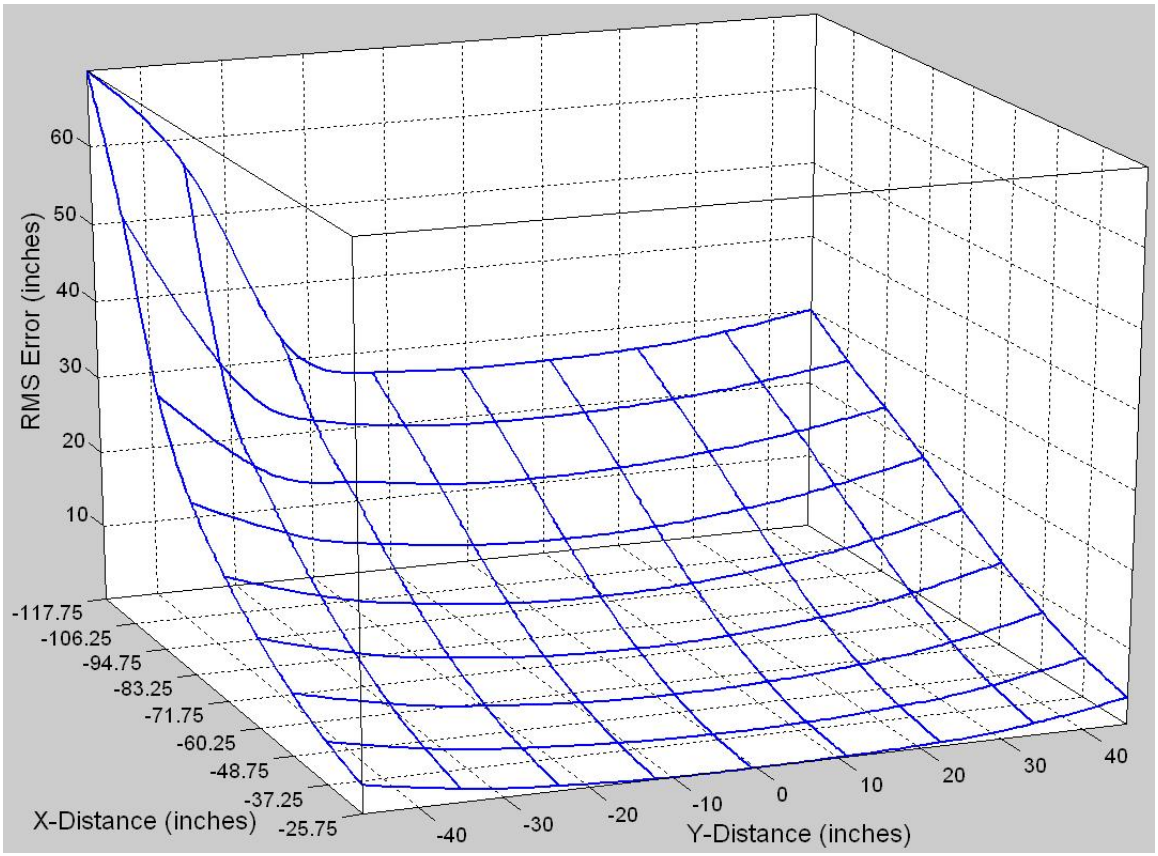

Figure 9.8: RMS Error Surface at Z = -32.75 Inches

9.2.7 Error Convergence Study

Upon completion of the first calibration, it was necessary to determine if the trends depicted in the error surface plots were truly representative of the error over the entire area. To either prove or disprove this theory, it was necessary to run a second calibration in order to verify these error trends. This second calibration was run by collecting data points at a distance of one fourth the previous calibration resolution in the X and Y directions, covering one fourth of the previous calibration in terms of total area. This calibration with a finer mesh grid proves that the error trends have a large

wavelength over the entire tracking volume; they do not oscillate rapidly between small distances. The fine mesh calibration's error surface was calculated and superimposed on the previous coarse calibration's error surface, see Figure 9.9.

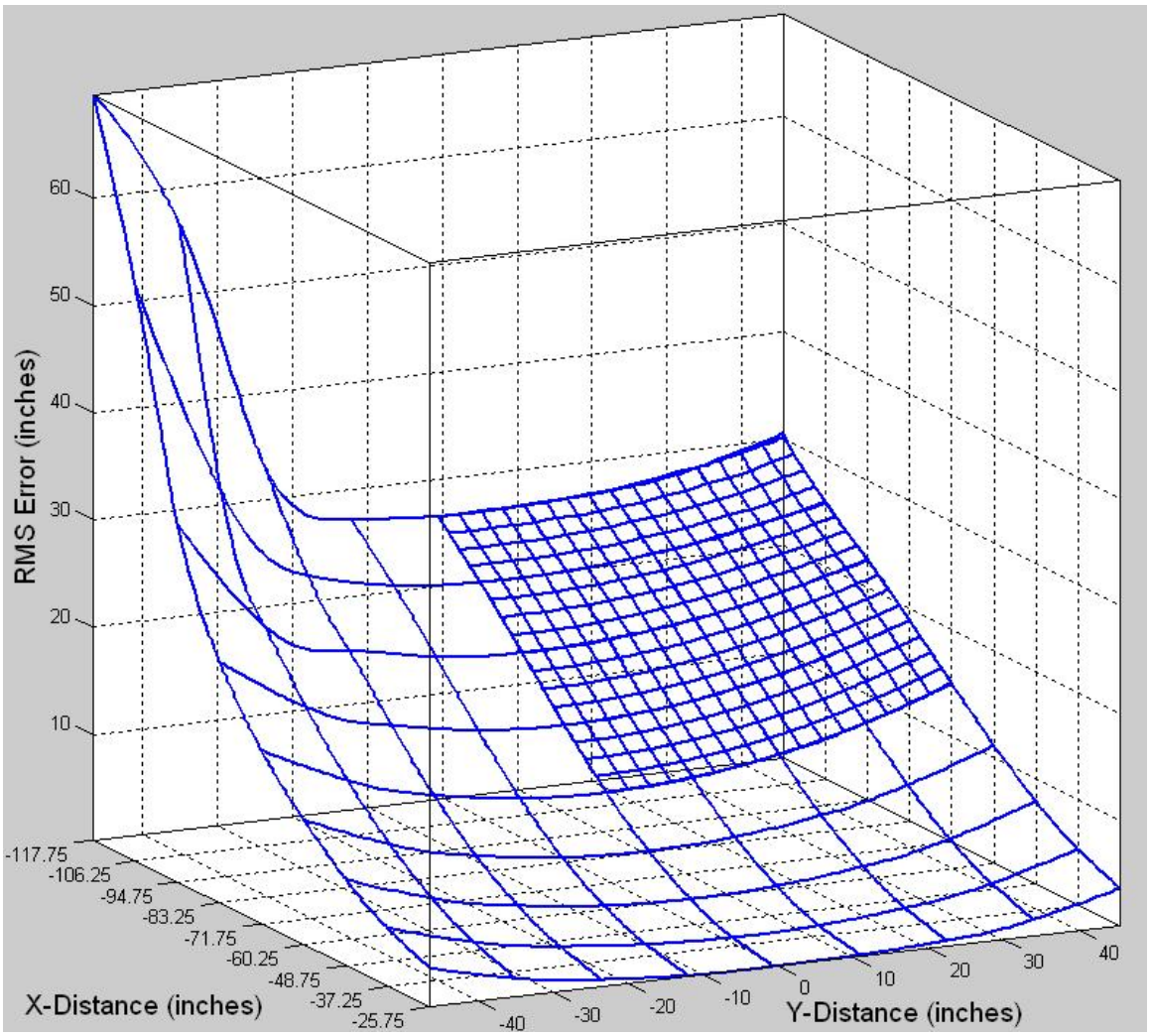

Figure 9.9: Fine Mesh Error Surface

The data points from the second calibration with 2.875" grid spacing fit directly onto the error surface from the first calibration with 11.5" grid spacing. There are some very slight discrepancies between the two plots, but they are only noticeable at the furthest possible distance from the transmitter (where distortion is greatly magnified). To further investigate these discrepancies, the RMS error at the 10' location in the X direction was

plotted as a function distance in the Y direction. This graph, Figure 9.10, provides a worst-case scenario for distortion oscillation between the two calibrations.

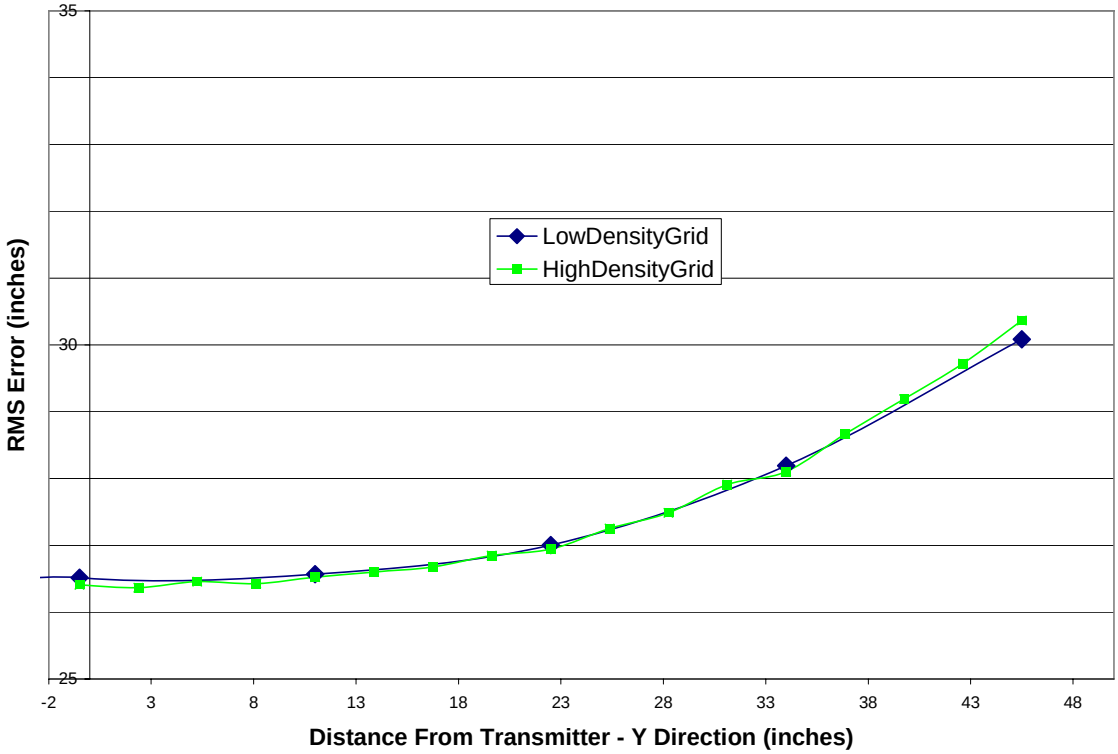

Figure 9.10: Distortion Oscillation

The maximum error between the first and second calibrations for any data points is 0.35" RMS at the farthest range of the transmitter. Therefore, a grid spacing of 11.5" is more than sufficient for applications requiring accuracy of less than 1". However, a higher grid density is necessary for ergonomics applications requiring 1 mm accuracy.

10. Conclusions and Future Work

A calibration device has been designed and manufactured to accurately position a receiver for an electromagnetic tracking system over a 16'x8'x6.5' range of motion. The device positions the receiver at user-defined grid points in order to calculate the error vectors at each location due the static magnetic distortion in the tracking environment. This automated device will allow an engineer to calibrate a region with very fine grid spacing while eliminating the previously time-consuming calibration process. The calibration data can be used to correct tracker readings in real-time to improve the performance of the tracking system for virtual reality applications.

Accuracy:

The most important factor in the construction of the calibration device was the positional accuracy. The goal for accuracy was 1mm, as stated in the original specifications from PACCAR. This goal has been met for each axis: 0.975 mm in the X and Y axis due to the 0.004 inches/inch accuracy of the lead-screw driven rails, and 0.003973 mm in the Z axis corresponding to the accuracy of the micro-stepping drive system for the telescoping arm. Any additional error in position can be limited by precisely measuring the starting "home" position of the bird.

Automation:

The calibration device was successfully integrated with the COVE software, to allow for automated data collection. Once the user has defined a region's grid points, motor commands are sent via serial port to the motor controller. The stepper motor drive

system translates the receiver to each grid point, pauses to collect data, and continues until all data has been collected.

Collision Avoidance:

Collision avoidance has been integrated into the COVE software. A completely modifiable CAD model is used to determine obstructions in the calibration space. The obstructions are calculated by converting the CAD model into a list of triangles. The vertices of the triangles are check to determine their proximity to the grid points. If the surface is within a given tolerance, the height is checked using a z-buffer sort to calculate the maximum height that the telescoping arm may descend during data collection. This ensures that the calibration device will not collide with obstructions in the tracking environment; the device will move around any obstruction and skip the grid points inside of its volume.

Time Benefits:

This device has greatly benefited the engineer in regards to the time required for collecting calibration data. The calibration time for this device can be split into two key components: setup time and collection time. The setup time takes less than five minutes for the engineer to initialize the device for data collection, and the collection time is dependent on the number of grid points. An array of 9x9x7 grid points collected over a very large 8'x8'x6' volume took less than three hours from start to finish, with no user intervention beyond the initial setup time. In comparison, the previous automated traverse from the preliminary research phase required eight hours for an array of 8x9x8 grid points collected over a small 2'x2'x2' volume. This preliminary research time required the constant interaction from two users to send the appropriate commands to the

motors as well as input the data into COVE. Early manually positioned calibrations such as the one performed by Gowda required approximately twenty seconds to accurately collect data at a single calibration point [10]. Using this benchmark, collecting a 9x9x7 array of grid points would have taken 189 hours with constant attention from the engineer.

Error Convergence:

Now that the calibration process is automated, it is very easy to collect multiple data sets. This could be very useful for researching further error convergence studies. One possible area of interest would be to develop an adaptive grid density program. This program would record the necessary accuracy in given regions for the tracking environment and output its associated grid density. This would require extensive calibrations with varying grid densities in order to fully define the benefits of decreasing the distance between grid points. This research has made such intensive data collection possible, as we can simply send a region file to an engineer at PACCAR who can then have the device automatically collect the data for analysis with minimal interaction.

Future Work:

Designing a cable management system for the device would be beneficial for future use. Currently the wires are routed above the frame and allowed to hang down where necessary, Figure 10.1. The existing method for cable management is to manually reel in the wires when the device is at the home position and then allow them to be dragged along with the device as it moves farther away. Incorporating cable carriers would eliminate the possibility of a wire getting bound during a traverse of either the x or y axis. Designing a system to wrap up the bird cable as the telescoping arm retracts and routing it through the cable carriers would also eliminate the possibility of the bird cable

becoming caught on obstructions in the tracking environment. This would require the purchase of an extended 50’ bird cable.

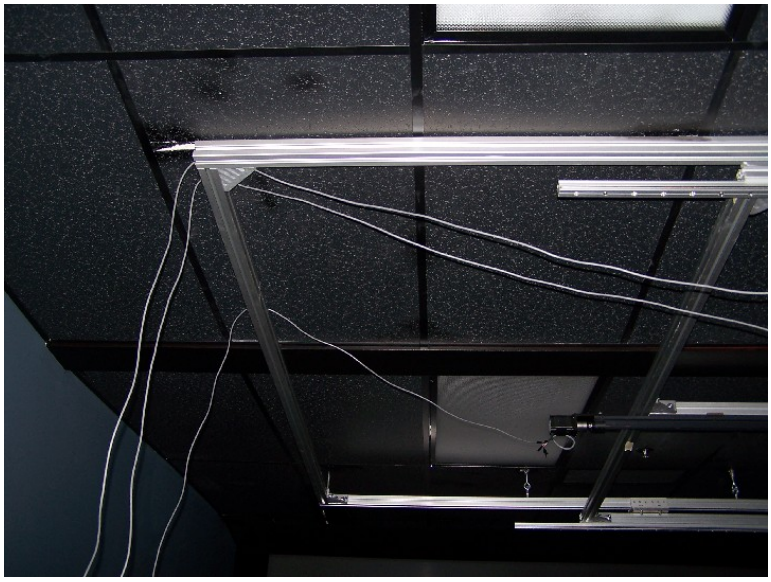

Figure 10.1: Cable Management

Another improvement to the design would be to re-evaluate the hanging weight. Currently the weight simply rises and falls opposite to the receiver, thus when the telescoping arm is retracted the weight is swinging close to the floor. While the weight is free to rotate about both its support on the sprocket as well as at its hinge connection with the chain, it may be possible for the weight to become caught on obstructions during calibration. If the weight is deflected by an object it can start to oscillate and in some circumstances bump into the telescoping arm, causing the arm to deflect slightly. Extending the plastic chain and fixing another sprocket or pulley on one end of the traverse would keep the weight out of the calibration environment and away from the telescoping arm. This pulley would have to be mounted to either the existing linear bearing for the x axis or on another linear bearing mounted to the smaller frame.

BIBLIOGRAPHY

[1] "virtual reality." *The American Heritage® Dictionary of the English Language, Fourth Edition*. Houghton Mifflin Company, 2004. 14 Feb. 2007. http://dictionary.reference.com/browse/virtual reality

[2] Immersion Corporation. http://www.Immersion.com

[3] SensAble Technologies. http://www.sensable.com/haptic-phantom-desktop.htm

[4] Ascension Technology Corporation. http://www.ascension-tech.com/products/flockofbirds.php

[5] Polhemus. http://www.polhemus.com/?page=Motion_Fastrak

[6] Nixon, M. A., McCallum, B. C., Fright, W. R., Price, N. B. (1998). The Effects of Metals and Interfering Fields on Electromagnetic Trackers, Presence, Vol. 7, No. 2, pp. 204-218.

[7] Kindratenko, V. (2000). A Survey of Electromagnetic Position Tracker Calibration Techniques. Virtual Reality: Research, Development, and Applications, Vol. 5, 2000, pp. 169-182.

[8] Repp, R. Calibration and Performance Characteristics of Virtual Reality Tracking Systems for Engineering Applications. Master's Thesis, Washington State University, 2000.

[9] Jayaram, U., Repp, R. (2002). Methods To Achieve Real-Time Calibration of Virtual Environment for Engineering Applications and Accuracy/Execution Time Tradeoff Studies. ASME Journal of Mechanical Design, 124(4), pp. 623-632.

[10] Gowda, S. The Calibration of Virtual Prototypes for Engineering Design and Analysis. Master's Thesis, Washington State University, 1996.

[11] Bryson, S. T. (1992). Measurement and Calibration of Static Distortion of Position Data from 3d Trackers. In Proceedings of SPIE Conference on Stereoscopic Displays and Applications III, volume 1669, pp. 244-255.

[12] Hagedorn, J., Satterfield, S., Kelso, J., Austin, W., Terrill, J., Peskin, A. (2005). Correction of Location and Orientation Errors in Electromagnetic Motion Tracking. National Institute of Standards and Technology, submitted. http://math.nist.gov/mcsd/savg/papers/Tracker.Presence.pdf

[13] Borst, C. W. (2004). Tracker Calibration Using Tetrahedral Mesh and Tricubic Spline Models of Warp. In Proceedings of the IEEE 2004 Virtual Reality Conference, pp. 19-26.

[14] Ghazisaedy, M., Adamczyk, D., Sandin, D., Kenyon, R., DeFanti, T. (1995). Ultrasonic Calibration of a Magnetic Tracker in a Virtual Reality Space. In Proceedings of the IEEE 1995 Virtual Reality Annual International Symposium, pp. 179-88.

[15] Livingston, M., State, A. (1997) Magnetic Tracker Calibration for Improved Augmented Reality Registration. Presence, vol. 6, no. 5, pp. 532-546.

[16] Nakada, K., Nakamoto, M., Sato, Y., Konishi, K., Hashizume, M., Tamura, S. (2003). A Rapid Method for Magnetic Tracker Calibration Using a Magneto-Optic Hybrid Tracker. MICCAI 2003. Lecture Notes in Computer Science (2879), Springer-Verlag, pp. 285–293.

[17] Henrich, D., Cheng, X. (1992) Fast Distance Computation for On-line Collision Detection with Multi-Arm Robots. In Proceedings of the IEEE Conference on Robotics and Automation, pp. 2514-2519.

[18] "Z-buffering." *Wikipedia, The Free Encyclopedia*. 29 Mar 2007. Wikimedia Foundation, Inc. http://en.wikipedia.org/w/index.php?title=Z-buffering&oldid=118780551.

APPENDIX A

SOLE SOURCE MEMO

WSU - VRCIM Lab

Memo

To: Purchasing Department

From: Sankar Jayaram

Date: May 1, 2007

Re: Justification for Sole Source Procurement of Equipment

Scope of Work:

The Virtual Reality and Computer Integrated Manufacturing Laboratory is in the process of designing an automated three axis Cartesian positioner to calibrate a magnetic tracking system. The tracking system encounters position error due to metal in the environment as well as increased distance from the transmitter. The goal of the calibration is to be able to position the receiver at known locations in specified increments throughout the virtual environment to measure position error as a function of location. The area to be calibrated is an 8'x8'x8' cube.

Minimum Requirements:

We need to purchase two linear actuators, each with an 8' travel length, to provide x-y translation. This calibration device requires a very accurate positioning system with less than 1mm accuracy over the entire travel length. The actuators must be able to position a minimum 50 LB payload to account for a third axis that is to be manufactured and installed here at WSU.

Compatibility Issues:

The system must be powered using standard size NEMA frame stepper motors. A three axis stepper motor controller system is being purchased separately in order to communicate via serial port with a computer. The control system is the Allegra programmable controller provided by OES Incorporated, viewable at http://www.oesincorp.com/allegroseries.htm.

Market Analysis:

We have contacted multiple motion control companies with regards to this device. Most companies do not manufacture linear actuators suitable for the application due to its extended traverse length. We have been able to find three companies that provide a suitable product:

- H2W Technologies
- Olympic Controls
- Pacific Machine Automation

The actuator from Olympic Controls did not have the required accuracy of less than 1 mm over the travel length. It is a belt drive design that is cheaper but has an accuracy of 2.5 mm over the travel length. This actuator would there need a linear encoder, consisting of a sensor and linear scale. This option requires a more expensive servo motor that can read the input from the linear encoder to provide accurate positioning. Programming software to control this system would be much more difficult than simple stepper control. This option would provide very good accuracy but is too expensive due to the complicated controls.
The actuator from Pacific Machine Automation is lead screw drive. It has the required accuracy and travel length but the price quoted was much too expensive at $3,721 each.

Recommended Acquisition:

The actuators from H2W are the best option for this calibration device. The design consists of a lead screw driven payload powered by NEMA 23 frame stepper motors, which are compatible with the Allegra control system. They have an accuracy of 0.004 inches/foot, corresponding to a total accuracy of less than 1 mm over the travel length. The price quoted was $2,400 per actuator.
We recommend a sole source purchase from H2W because their devices are the only ones that meet our accuracy, price, and size requirements.